Alma Mater Studiorum – Università di Bologna

DOTTORATO DI RICERCA IN

GEOFISICA

Ciclo XXV

Settore Concorsuale di afferenza: 04/A4

Settore Scientifico disciplinare: GEO/10

TITOLO TESI
LOCATING SOURCE OF VOLCANIC TREMOR AT STROMBOLI VOLCANO, ITALY

Presentata da: **MARIANTONIETTA LONGOBARDI**

Coordinatore Dottorato   **Relatore**

PROF. MICHELE DRAGONI   **DR. LUCA D'AURIA**

Esame finale anno 2013

Index

Introduction

The purpose of this work is to develop a method for locating volcanic tremor sources. This method will be applaied on Stromboli vulcano dataset (7 years of recods). The work will concentrate mostly identifyng the number and location of the sources investigating on their temporal variation.

Volcanic tremor has attracted considerable attention by seismologist because of its potential value as a tool for forecasting eruptions and better understanding the physical processes that occur inside active volcanoes. However, unlike tectonic earthquakes where the dominant source process is brittle failure of rock, the driving mechanism of tremor seems to involve complex interactions of magmatic fluids with the surrounding bedrock. These interactions are responsible for the following distinct characteristics found in volcanic tremor recorded at many volcanoes worldwide: a) the onset of tremor may be emergent or impulsive, with its amplitude showing in many cases a dirct relationship the volcanic activity; b) in the frequency domain the spectra consist of a series of sharp peaks in the band 0.1-7 Hz, representing either a fundamental frequency and its harmonics, or a random distribution, while quite often they exhibit temporal variations in their content; c) the depth of the source can very considerably from one volcano to another in the range of a few hundred metres to 40 km; d) tremor may occur prior to and/or after eruptions with a duration that ranges from several minutes to several days or months. The methods used to study tremor include spectral analysis using both the Fast Fourier

Transformation and the Maximum Entropy Method, polarisation analysis of the wavefield and methods that make use of array data to deduce the backazimuth and type of the seismic waves as well as the location of the source. Visual and/or recorded acoustic observations of the ongoing volcaanic activity have assisted in many cases to further constrain proposed physical mechanisms for the generation of tremor. The models suggested as possible sources of tremor can be grouped as follows: a) fluid flow induced oscillations of conduits transporting magmatic fluids; b) excitation and resonance of fluid-filled cracks; c) bubble growth or collapse due to hydrothermal boiling of groundwater; d) a variety of models involving the oscillations of magma bodies with different geometries. It has been proposed by many authors that the source of tremor is not unique and may differ from one volcano to another, a fact that adds mor difficulty in the source modelling efforts.

Most methods used to locate volcanic tremor sources are: 1) use of array, 2) the calculation of wave field amplitude. The study on volcanic tremor for Stromboli volcano will be carried out adopting the latter basing the method on a realistic wavefield model.

1 Chapter

Volcanic Tremor

1.1 General Consideration of Volcanic Tremor

Volcanic tremor that occurs the eruptions of volcanoes is one of the most interesting phenomena characterizing the dynamics of eruption. Whereas volcanic-tectonic earthquakes (Gorshokov, 1954) principally do not differ from ordinary tectonic ones and volcanic (explosive) earthquakes have many common features with powerful explosions, volcanic tremor seems to be a unique phenomenon that has no correspondences with any other phenomena being studied with seismic methods.

Volcanic tremor was recoded for the first time during the Usu volcanic eruption (Omori 1911) in 1910 and after that was recorded repeatedly during the eruption of volcano Kilauea (Eaton and Richter, 1960; Finch, 1949), Mauna Loa (Finch, 1943; Jaggar, 1920), Krakatau and Paricutin (Finch, 1949), Vesuvius (Imbo, 1935), Meakan-dake (Sakuma, 1959).

In the course of seismic investigation of volcanic tremor, some regularities were found that characterize this process, the principal ones of which are as follows: 1) stability of volcanic tremor in time (from 2-3 days to several months) (Gorshkov, 1954; Finch, 1943, 1949; Jaggar, 1920; Omori, 1911), 2) stability of the period and the amplitude of tremor (Gorshkov, 1954; Finch, 1949; Macdonald, 1952; Sakuma, 1957).

In most of the above mentioned papers the authors have supposed in the obvious form that the volcanic tremor is provoked by the displacements of

masses in the deep or near surface parts of volcano apparutus. So, a nonstationary source was suggested as the cause of a time stationary phenomena. In particular, Fincher (1949) supposed that the source of volcanic trembling on Hawaii was "rhythmic shock activity of rising lava". However, from the geological and seismological points of view one cannot imagine such a mechanism of "tectonic-magmatic generator" that forces the pillar of lava some kilometers high to pulsate with the stable frequency and amplitude for some weeks or even some months.

In other papers, leakage of gases trhough the system of cracks (Sakuma, 1959), and the movement of magma in the channel were taken as possible sources of volcanic tremor.

Volcanic tremor is, as previously noted, always a sign of high activity. However since the exct mechanisms are still unknonw, the importance and timing between the first appearance of tremor and possible eruptive activity is sill a matter of discussion (McNutt, 2000a).

1.1.1 Tremor Frequency Distributions

The mean and median frequencies are both near 3.5 Hz, and 90% of the data lie between 1 and 9 Hz. It is often observed that tremor frequencies are relatively insensitive to changes in azimuth or small changes in distance (attenuation becomes important only over large distances).

1.1.2 Duration

One of the most basic pieces of information about a tremor episod is its duration. Figure 1 shows a histogram of tremor durations for two samples, 488 cases from a single volcano, Pavlof (Alaska), and a worldwide sample of 1100 cases from 84 volcanoes. Short-duration episodes, those lasting minutes to hours, account for 93% of the Pavlof sample and 80% of the worldwide sample. The two distributions roughly mimic each other, that is, a single volcano and a large group of volcanoes share common features. Most of the long-duration tremor episodes, those lasting weeks or longer, accompany long-duration eruptions.
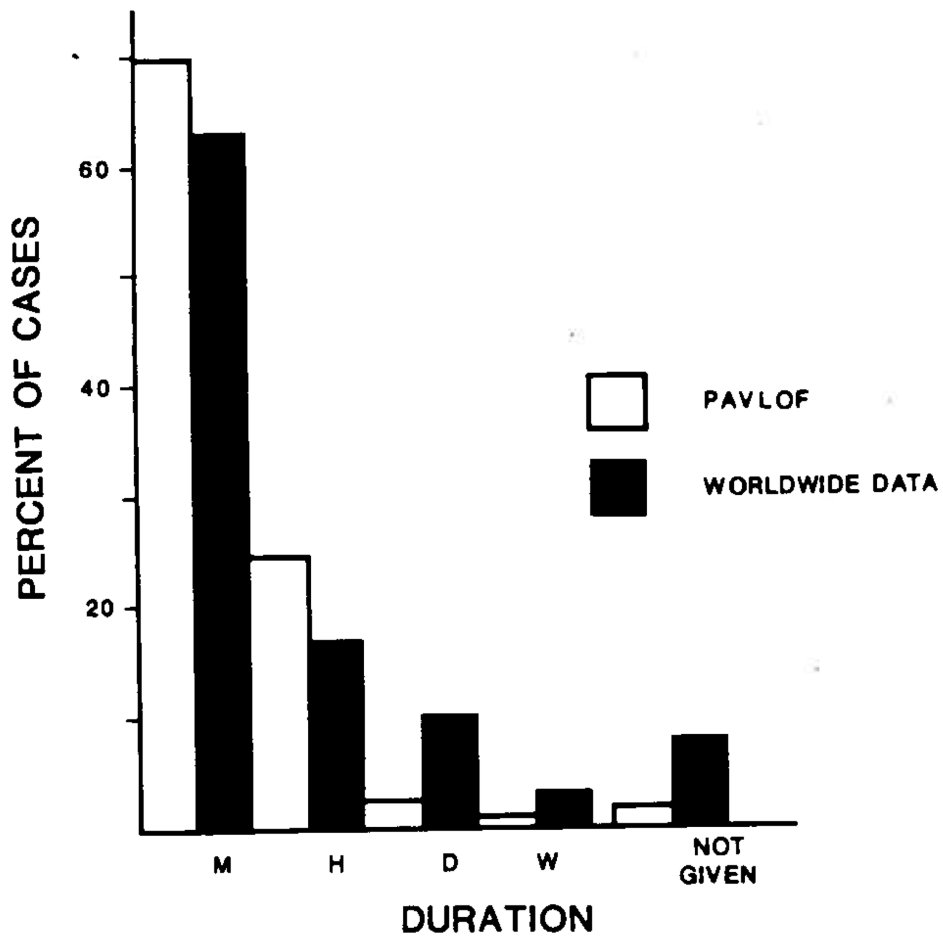
Fig.1. Volcanic tremor durations for 488 cases from Pavlof Volcano and for a worldwide sample of 1100 cases from 84 volcanoes. Heights of bars are proportional to percentage of total data sample. Times are 2-59 min (M), 1-23 h (H), 1.6 days (D), and 1 week or longer (W).
(From S.R. McNutt, 1987)

1.1.3 Aplitudes

It normalizes or standardizes the amplitudes to a common reference. This is essentially the same type of solution used in the determination of earthquake magnitudes. A normalization called reduced displacemente (R.D.) is widely used. There are two formulas. For body wave (P- waves and S-waves):

$$R.D. = \frac{A \cdot r}{2\sqrt{2} \cdot M}$$

For surface waves (Rayleigh waves, Love waves. And PL waves):

$$R.D. = \frac{A \cdot \sqrt{\lambda r}}{2\sqrt{2} \cdot M}$$

Where A is amplitude in centimeters peak-to-peak, r is distance from source to seismic station in centimeters, M is sismograph magnification at the tremor frequency, and λ is wavelenght in centimeters. The $\sqrt{2}$ term is a correction for root mean square (rms) amplitude, assuming that most tremor resembles a sinuisod. The formulas correct for the effects of geometric sperading, instrument magnification, and rms amplitude, but not for attenuation. Both formulas were mathematically derived from the far-field expressions for displacement at a point source. The surface wave formula explicitly includes the wavelength. The normalization distance is

1cm, which is essentially at the source. The unit of reduced displacement are cm^2. A seismic station that can record earthquakes of magnitude 1.0 will also record tremor of 2.2 cm^2 reduced displacement at 3 Hz. For each increase of one earthquake magnitude unit, the reduced displacement increases by a factor of 10. (Seismology, Theoretical.)

1.1.4 Special Cases: A. Banded Tremor

"Banded" tremor occur in regular, periodic bursts separated by quiescence of uniform duration. The resulting pattern looks like stripes or bands on seismograms. The degree of regularity is partly a function of the speed of revolution of the seismograph drum. If the duration of the tremor signal or quiescent period is an integer multiple of the period of revolution, then the tremor will appear exactly banded. If the two are dissimilar, the signal will appear irregularly banded. Most examples of banded tremor have been recorded during times of hydrothermal activity, suggesting that the tremor may be caused by cavities refilling at a uniform rate and then boiling off. The magmatic cases suggest flow at uniform rate into a shallow magma body that eruption when some critical capacity or strength is exceeded.

B. Spasmodic Tremor

Most tremor looks like an irregular sinusoid with frequencies between 1 and 5 Hz. A second type of tremor, called spasmodic tremor, consists of pulses of high frequency, usually 5-10 Hz or more. In some cases, the pulses are discrete earthquakes producing separate P-waves and S-waves. In others the seismograms are phaseless. The signal is continuous in the sense that new subevents occur before the coda of the previous subvent returns to background levels (Fig. 2). Spasmodic tremor has been recorded at Kilauea, Mount. S. Helens. Although this type of tremor has only been

recorded at a small number of volcanic areas, no signals like these are known from nonvolcanic areas. The presence of fluids has been suggested as a contributing cause of spasmodic tremor, since fluids would increase the pore pressure and lubrificate fault surface.

Typical Earthquake

19 July 1989 0752 GMT

M ≈ 1.1 DEPTH ≈ 4.5 km

Spasmodic Tremor

27 July 1989
0334 GMT

0   10   20   30   40   50   60

TIME (SECONDS)
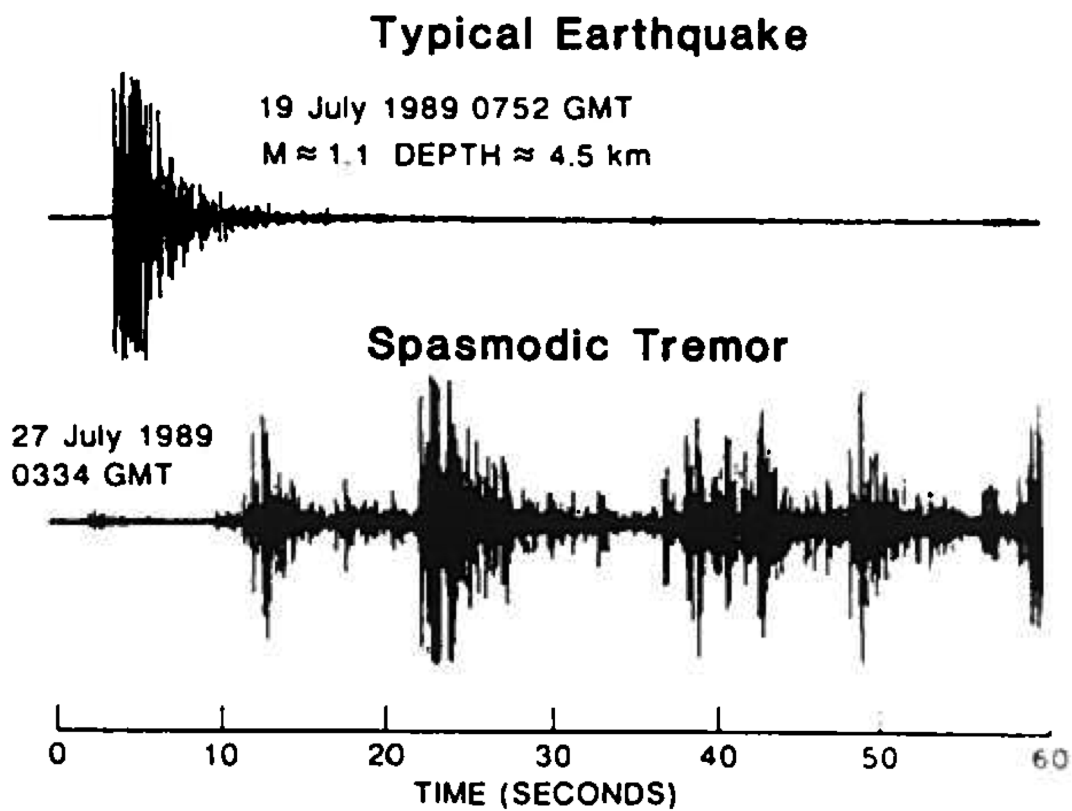
Fig. 2. Seismograms of a typical earthquake and typical spasmodic tremor at Mammoth Mountain, Calfornia. The spasmodic tremor burst has overlapping coda of small earthquakes and high background signal level that persist beyond normal coda decay times.

C. Deep Tremor

Most tremor originates at shallow depths (0-5 km), but deep tremor or deep LF events occur repeatedly at Kilauea at depths of 30-60 km. The durations of these episodes rarely exceed 1 h. Deep LF events are known at Izu-Oschima (Japan) where a single monotonic LF event occurred at a depth of 30 km, at Lassen Peak (California) whre about one dozen long-period events between depths of 16 and 22 km were recorded, and at Mammoth Mountain, where a sigle LF event at a depth of 18 km was recorded.

2 Modelling the source of volcanic tremor

The process of how magma ascends from a deeper source and moves towards the surface causing an eruption has been studied extensively by many authors and at different scales. On the smallest possible scale magma is considered to flow through the porous matrix of partially molten rock, forming during its ascent shape-preserving waves as has been demonstred analytically (Scott and Stevenson, 1984) and experimentally (Scott and Stevenson, 1986). On a larger scale, the interior of a volcano is modelled as consisting of a shallow magma reservoir fed by a deeper source and a cylindrical-shaped conduit that transports the fluid upwards and may be connected to a network of other conduits (Fedotov,1981). In general the reservoir is considered to behave elastically under variable stress conditions imposed by fluid accumulation or outflow. The cylindrical conduit on the oder hand is believed to exhibit more complicated, viscous behaviour so that a high driving fluid pressure from below results in deformations transmitted periodically as expansions or contractions of its wall (Ida and Kumazava, 1986; Ida, 1996). Elastic behaviour of the conduit may also be expected when the fluid pressure builds up quikly, forcing the conduit to respond elastically by a fast opening (Maeda, 2000).

Several observations made during eruptions seggest a direct link between inward and outward flow of magma from a reservoir and the generation of volcanic tremor. Tilt observations indicate the occurence of cycles of slow build-up of ground dformation starting as volumetric expansion and terminating with contraction, being accompanied almost always by tremor

episodes (Kilauea Dvorak and Okamura, 1985; Izu Oshima Oikawa et al., 1991; Fukao et al., 1998).

2.1 Resonance of large magma bodies

Among the first model to be used in order to explain the occurence of volcanic tremor is that of the free oscillations of magma bodies of various shapes. For example Sassa (1936) and later Shima (1958) and Kubotera (1974) suggested that the observed 10-s-period tremor at Mt. Aso was caused by the oscillation of a spherical magma chamber beneath the volcano. Assuming that the low-frequency earthquakes may be a kind of impulse response of the tremor-generating system, Chouet (1985) proposed a model to explain such earthquakes by studing the oscillations of a buried magmatic pipe. The pipe consisted of three parts: on the top a hemispherical cavity filled with gas was considered to be triggering the oscillations due to excess gas pressure, in the middle the resonating pipe had a cylidrical shape and was filled with magma, and at the bottom it was shut by a horizontal disk. The calculated free surface response of this system showed an impulsive signature in the vicinity of the pipe, but evolved to harmonic wavetrain at larger diastances. Based on similar ideas about the relationship of tremor and low-frequency earthquakes, Crosson and Bame (1985) studied the resonance of a magmatic filled spherical cavity encased in country rock which contained a smallar cavity filled with gas. The motivation for such a model also came from observations at Stromboli, where low-frequency earthquakes were found to originate a few seconds prior to exsplosions. In that sense expansion of the gas-filled cavity could set the magma-filled one into resonance. The signal generated by such an oscillation had a frequency content of 1-5 Hz, consistent with the observations, and an impulsive signature in the time domain. Again it

was assumed that sustained expansions of the gas-filled pocket (probably due pressure variations) would give rise to continuous tremor.

2.2 Hydrothermal boiling

The fact that the formation of bubbles in a liquid is an efficient way of seismic energy generation has long been recognised and utilised in exploration geophysics (Dobrin and Savit, 1986). Gysers and geothermal reservois are natural sources of such seismic energy and seismological studies at the Old Faithful geyser revealed the existence of tremorlike signals related to boiling of ground-water (Kieffer, 1984; Kedar et al., 1996). Leet (1988) suggested that processes similar to the ones observed at Old Faithful could be used to explain the generation of volcanic tremor recrded during quiet periods at certain volcanoes, which he called "non eruption tremor". Two restrictions regarding this model are: a) the magma chamber underneath the volcano acting as the source of heat should not reside at higer elevation level than the groundwater table; and b) the process should operate at shallow depths, so that steam can be separated from the liquid. Obviously, hydrothermal boiling cannot explain tremor processes operating at depths larger than a few kilometres from the Earth's surface. Boiling of graundwater causes the formation and growth of bubbles in the liquid that may collapse if they encounter a liquid ragion of lower temperature. Either of these two mechanisms can generate seismic energy, but Leet (1988) found that bubble collapse is 10^2 - 10^4 times more efficient in converting thermal power to seismic power; the boiling heat transfer rates in order for bubble collapse to generate 1-Hz tremor should be about 1000 MW, which he notes is the upper limit of observed heat flow in volcanic crater lakes and geothermal areas. The resulting signal is expected to resemble white noise, with equal energy in all

frequency bands, which is in contrast to the sharply peaked tremor spectra.

2.3 Excitation of fluid-filled cracks

Brittle failure of rock and crack formation inevitably accoompany any upward movement of magma during different stages of volcanic activity. The main result of such rock fracturing is the generation of various types of seismic signals, ranging from events that can hardly be distinguished from common tectonic earthquakes to low-frequency events with emergent onsets, absence of clear S-wave phases and a slowly decaing coda Chouet, 1996). Injection of water into hot dry rock has been found to produce seismic signals similar to low-frequency volcanic earthquakes and supports the idea of a source that involves the opening of tensile cracks caused by excess fluid pressure (Bame and Fehler, 1986). The overall similarity of tremor and low-frequency events in the time and frequency domains, notwithstanding their different signal has been pointed out by many authors as indicating that a common source may be at work, and which of the two seismic signals will be generated depends on the duration of the excitation mechanism (Fehler, 1983; Chouet, 1985; Hofstetter and Malone, 1986; Tsuruga et al., 1997; Almendros et al., 1997). Volcanic tremor underneath Kilauea during the 1963 eruption was mainly composed of P waves, shared the same source area with the low-frequency eartquakes and was deep enough to assume that the observed tremor could be explained by the magmatic pressure build-up as magma moves away from a deep reservoir beneath the summit of the volcano. The cracks may be placed in a series and are connected by narrow channels that open when magma pressure reaches a critical value, facilitating the movement of fluid from one crack to the next one. The vibration caused by such a movement

was found to have a period proprtional to the crack length and amplitude that depended on the excess pressure and the area of extension. In order to explain the temporal variations of the frequency content during a tremor episod from higer (5-10 Hz) to lower frequenzies (1.5-3 Hz), Aki and Koyanagi (1981) suggested that this process starts with a few cracks generating a signal of small period which increases as more cracks vibrate and the length of the chain gets longer. However, two descrepancies have been pointed out regarding this model; first, as the length of the chain is increasing, thisshould lead to sustematic lowering of the frequencies of the length of the chain is increasing of the tremor signal, which was not observed. Second, numerical studies on crack generation and growth show that a tensile stress regime combined with the fact that the largest part of each crack is expected to be filled with fluid, favour catastrophic growth rather than a stable opening-closing process (Sammis and Julian, 1987). Chouet (1986, 1988) considered the displacement of the walls of a fluid-filled crack (Fig. 4) caused by a pressure disturbance in the fluid as a possible model for the generation of low-frequency earthquakes, as well as tremor, if the disturbance is sustained. This model is qualitatively different from that proposed by Aki et al. (1977), since it assumes the vibration of only one crack with no inflow or outflow of fluid taking place. The caracteristics of the far field wavefield radieted by a rectangular shaped vibrating crack, filled with an inviscid fluid and assuming that the surrounding bedrock behaves as a Poisson solid, were found to depend on the following parameters: a) the crack geometry; b) the position and the area over which the pressure disturbance occurs; c) boundary conditions for the stress on the crack's surface and the fluid flow at the crack

paramiter; and d) a dimensionless quantity called the crack stiffness C and the fluid-solid impedance contrast Z. Volcanic tremor underneath Kilauea during the 1963 euption was mainly composed of P waves, shared the same source area with the low-frequency earthquakes and was deep enough to assume that its source had to do with magma transportation rather than degassing processes (Aki et al., 1977; Aki and Koyanagi, 1981). Aki et al. (1977) proposed that the observed tremor could be explained by the jerky extension of a chain of cracks caused by magmatic pressure build-up as magma moves away from a deep reservoir beneath the summit of the volcano. The cracks may be placed in a series and are connected by norrow channels that open when magma pressure reaches a critical value, facilitating the movement of fluid from one crack to the next one. The vibration caused by such a movment was found to have a period proportional to the crack length and an amplitude that depended on the excess pressure and the area of extension. In order to explain the temporal variations of the frequency content during a tremor episode from higer (5-10 Hz) to lower frequencies (1.5-3 Hz), Aki and Koyanagi (1981) suggested that this process starts with a few cracks generating a signal of small period which increases as more cracks vibrate and the length of the chain gets longer. However, two discrepancies have been pointed out regarding this model; first, as the length of the chain is increasing, this should lead to systematic lowering of the frequencies of the tremor signal, which was not observed. Second, numerical studies on crack generation and growth show that a tensile stress regime combined with the fact that the largest fluid, favour catastrophic growth rather than a stable opening-closing process (Sammis and Julian, 1987). Chouet (1986, 1988)

considered the displacement of the walls of a fluid-filled crack caused by a pressure disturbance in the fluid as a possible model for the generation of low-frequency earthquakes, as well as tremor, if the disturbance is sustained. This model is qualitatively differnt from that proposed by Aki et al. (1997), since it summes the vibration of only one crack with no inflow or out flow of fluid taking place.
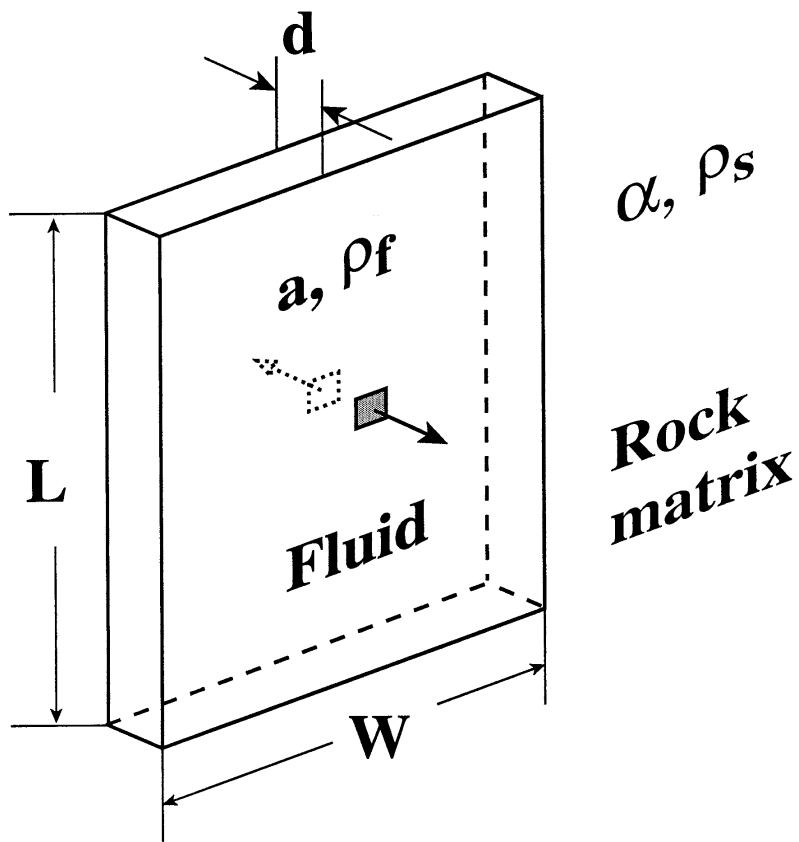
Fig. 3. Geometry of the fluid-filled crack model described by Chouet (1986, 1988). The shaded area indicates the place of application of the pressure transient thet triggers resonance.

2.4 Fluid-flow-induced oscillations

The quantitative study of magma flow through a geometrically irregular volcanic conduit poses a diffult numerical problem which requires the formulation and simultaneous solution of a system of partial differential equations describing the flow of the fluid as well as the elastic disturbance being caused by the coupling to the surrounding rock (Chouet and Julian, 1985). Futher complications may arise if the fluid consists of a gas and liquid phase, or if the thickness of the conduit changes in space as well as in time, effectively exhibiting viscous or visco-elastic behaviour. In models of tremor generation involving fluid flow, a number of simplyfing assumptions are usually made: a) the fluid has constant density and consists of one phase only, b) the motion occurs in one or two dimension and c) the conduit behaves elastically, while its thickness can only change as a function of time. Based on these assumptions and using the principles of conservation of mass and momentum for the fluid, Julian (1994) derived a third-order system of non-linear ordinary differential equations that describe the flow inside a verically extending crack connecting an upstream and downstream reservoir (Fig.3).

Another type of flow-induced oscillation may occur if the fluid system is suddendly perturbed from its equilibrium state by some external cause, like fracturing of the surrounding bedrock and formation of a new conduit, or a sudden variation in the fluid supply (St Lawrence and Qamar, 1979; Ferrick et al., 1982). This will result in the generation of a fluid transient with characteristics that will depend on the physical properties of the fluid, the geometry of the conduit and the boundary conditions. Pressure

oscillations caused by the transient will displace the conduit walls generating elastic waves in the surrounding medium.

More complicated behaviour is expected if the conduit is a part of an extended network such as is believed to exist beneath many volcanoes. Energy considerations show that once the system is perturbed it will continue to oscillate, until damped primarily by fluid friction, since dissipation of energy due to the generation of seismic waves is relatively small (Ferrick and St. Lawrence, 1984). Similar unsteady flow in cinduits followed by tremor-like seismic signals has been reported at a power plant at oroville, California caused by a faulty valve and at Tarbella dam, Pakistan, while water was moving through outflow tunnels (McNutt, 1986).
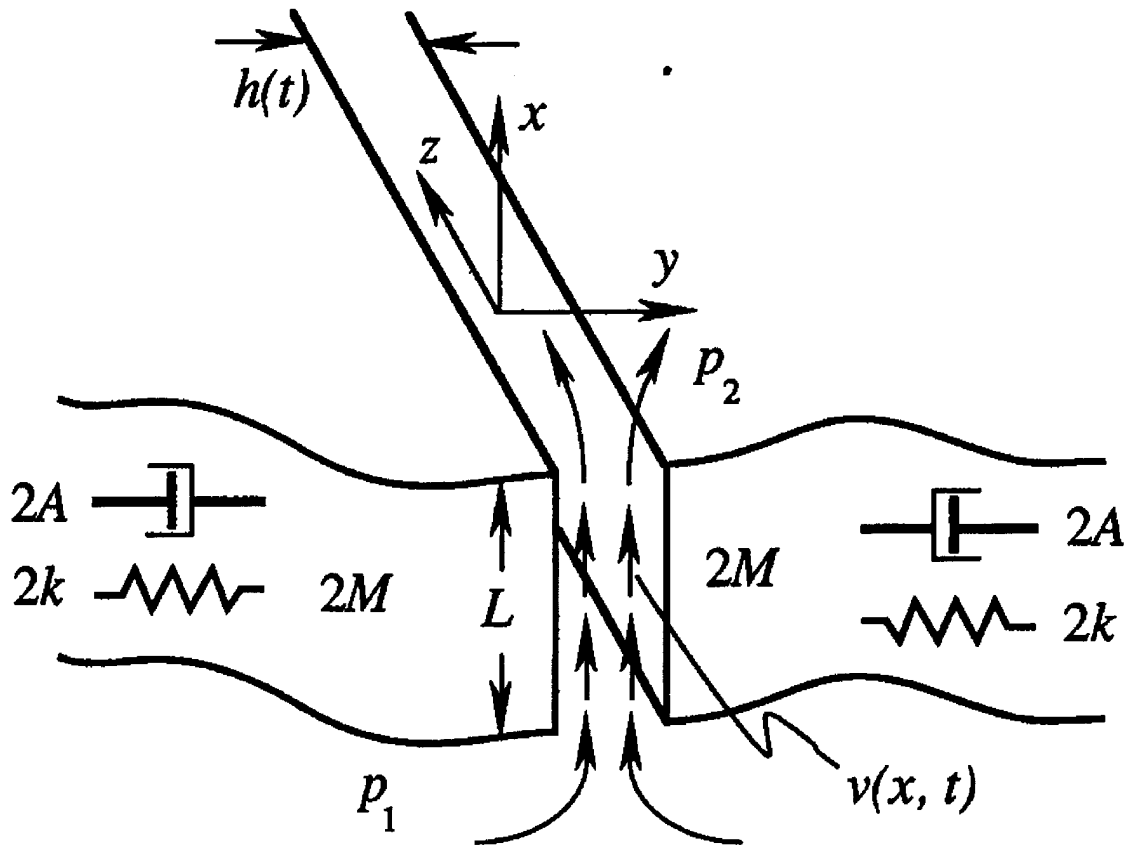
Fig. 4. Lumped parameter model of the generation of volcanic tremor. Viscous incompressible fluid flows in the x direction from the upstream to downstream reservoir through a channel of length (L) with imperfectly elastic walls, modelled as movable but underformable blocks of mass 2M, stiffness 2k and damping constant 2A (all measured per unit distance in the z direction). All motion occurs in the x-y plane and it is independent of z. The dynamic variables are the channel thickness h(t) and the fluid speed v(x,t) (from Julian, 1994).

3 Volcanic tremor at Kilauea volcano

Harmonic tremor characterized by an almost constant frequency pattern throughout the duration of its seismic signal is associated with eruptive activity and magma movement in Hawaii. The signal frequency is believed to vary inversely to the length of the generating source, and amplitude varies according to rate of magma movement under confining pressure. The eruption related tremor reflects high-frequency seismic and acoustic disturbance from lava-fountain activity. The amplitude of eruption tremor oscillates at intervals of a few seconds in a temporal pattern resembling that of intense lava fountaining, in which high bursts repeatedly occur seconds apart. This characteristic pattern may be related to pulsating magma movement driven by continual pressure fluctuations. Added to the eruption zone activity, tremor and long-period events that are localized at the summit vary in intensity according to the maagnitude and rate of the associated inflation-deflation episodes. Long-period events and tremor are inferred to share a common origin, and selected long-period events with identifiable onset times are locatable using standard earthquake locating techniques. The locations of long-period event may, in turn, be used to identify the source region of tremor beneath Hawaii and to further define depth-time classifications of tremor.

3.1 Harmonic tremor

Harmonic tremor, a seismic indicator of magma movement and eruptive activity, has been instrumentally documented at the Hawaiian Volcano Observatory (HVO) since 1912. It is identified on seismograms by a sustained signal that varies within a limited range of frequencies. Its duration is determined by the duration of volcanic eruption or of accelerated magmatic activity within the transpport system. At HVO, tremori s classified into three categories of inferred depth on the basis of relative amplitude and real extent of detection in the seismic network. Tremor is logged in terms of minutes per hour for short episodes and hours par day for longer events. Most of our tremor data is related to activity at Kilauea, since that is ehere most activity has occurred in the past 20 years and where our network of seismometers is densest. Seismic data collected from such prolonged Kilauea eruptions as the Mauna Ulu sequence in 1969-1974 and the Puu Oo sequence in 1983-1985, and from a significant southwest rift intrusion in August 1981 have provided a comprehensive record of shallow tremor associated with eruptions and intrusions, s well as, tremor associated with the aftermath of eruptive-intrusive activity or during periods of increased magmatic activity within the magma transport sustem at depth. Tremor near eruptive vents varies in amplitude according to the vigor of eruption. The seismic signal associated with eruption attenuates rapidly with increasing distance from the eruptive vent. Harmonic tremor that occurred in places or times unrelated to eruption is presumed to be associated with magma movement at depth. It is commonly localized beneath the Kilauea summit region at crustal depths but spreads to cover a large area beneath the active volcanoes in the south Hawaii region at mantle depths. Episodes of such tremor are often accompanied by increased numbers of long-period events, which have measurable onsets and travel tmes across the seismic network that fit P-wave velocities expected for normal earthquakes. The amplitude and signal duration of the long-period events vary like those of earthquakes, but otherwise their spectra resemble those of tremor in having consistently

peaked frequencies throughout the coda. Similarity of the distance-attenuation rates for the long-period events and for tremor further implies a common source or origin. If we accept a common origin for long-period events and tremor, then the precise determination of hypocenters for a sufficient number of long-period events accurately constrains the source region for tremor beneath Hawaii. The depth distribution of located long-period events as a function of time provides insight into the dynamic processes involved in the ascent of magma pluming system to eruptions of lava on the surface. Koyanagi and others (1976) have shown how swarms of short-period earthquakes outline the upper boundary of the shallow storage system beneath the summit of Kilauea and how a persistent source of long-period events defines the magmatic feeding sysstem below. A region in which few earthquakes occur, lacated at a depth of 3-6 km, is interpreted to be the storage zone of magma having an expected low rigidity. Swarms of shallow earthquakes and rapid changes in ground tilt during vigorous intrusions of magma are often accompanied by a background of low-amplitude tremor. Upon eruption of lava, the tremor amplitude increases and the frequency of earthquakes decreases. During the euption, the amplitude of tremori is influenced by lava movement and fountaining at the eruption site and by magma movement within the conduit sistem near the summit. Bursts of tremor at intermediate depths beneath Kilauea are occasionally recorded during eruptions, but these usually accompany gradual inflation of the summit. Persistent deep tremor in the mantle beneath south Hawaii had individual episodes that last one-half hour to several hours, and their cumulative reduced displacement as a function of time yields a rate of magma ascent from the mantle (Aki and Koyanagi,19981). Reduced displacement refers to the source intensity of tremor calculated from seismographically measured ground amplitudes.

3.2 The Mauna Ulu eruption in 1969

The Mauna Ulu eruption series was preceded frequency of shallow earthquakes in the summit region several weeks before and a subsequent increase in the number of east-rift earthquakes a week before the pre-eruption seismic swarm. The initial outbreak on May 24, 1969, started within hours of earthquake swarms and weak tremor in the east rift and deflation of the summit. Increased harmonic tremor occurred just before the lavaa outbreak on the east rift. After a two-week repose, activity renewed with long periods of quiescence persisted until the end of the year, producing 12 pronounced episodes of strong eruption. The intense fountaining episodes accompanied by high-amplitude tremor generally lasted less than a day; they were spaced at intervals varyng from several days to more than two months. Between the major episodes, low amplitude tremor was continous in the aerea of the active vents. The repeated pattern of eruption and accompanying sequence of tilt and seismic events is summarized in figure (Fig. 5). The nearness of th eruptive vent to the summit made it difficult to distinghish tremor possiblygenerated from separate sources along the conduit system during major episodes of eruption. Strong eruption tremor dominated at stations near the eruptive vents, as well as at those in the summit region. Gradual inflation and an increase in shallow earthquakes at the summit preceded the eruptive outbreaks. Shallow tremor at the eruption vent increased in aplitude simultaneously with the increase in lava output and fountaining. Abrupt onsets and endings these eruptive episodes were accompanied by equally rapid changes in tremor amplitude. Sustained high rates of summit deflation associated with the major eruptive outbreaks were followed by an increase in very small long-period events and harmonic tremor at the summit. Harmonic tremor sometimes developed into a fluctuating pattern, in which bursts of higher amplitude lasting 5-10 seconds occurred repeatedly and as frequently as several times per minute level of continuous tremor, and long-period events with higher amplitude and more definable onset times occurred at wide intervals of many minutes. The

areal variation of tremor amplitude is shown in figure 6 1-min samples of seismograms from temporary stations occupied with a jeep-mounted mobile seismic unit. This survey was made a few hours after a major eruptive episode in order to avoid seismic and acoustic noise from hugh fountaining and during a time interval when tremor amplitude remained fairly stable so that time difference had minimal effect on station-to-station comparisons. However, the sampling was intended to be soon enough after the eruptive episode to capture the expected stabilizing movement of magma within the conduit system following a major outbreak. The survey was repeated several times after major episodes of lava fountaning. For comparability, the tremor was recorded at the same instrumental gain at each station. Amplitude read from continously recording stations near the eruptive vent and in the summit area were used for reference. The comparisons of amplitudes in figure 7A and 7B generally indicate a persistent source at the active vent, and a secondary source at the summit caldera region, which decay to background after about a day of activity. Between major episodes of lava fountaining, when eruptive activity was limited to varyng rates of visible lava movement in the vent (Swanson and other, 1979), the amplitude of harmonic tremor recorded on seismographs within a few km of the vent changed according to the rate of lava movement. An example of time variation in tremor amplitude that correlated with a pattern of lava oscillation in the Mauna Ulu vent is shown in figure 8. High and low activity alternated at intervals of a few to many hours. During other intervals between major outbreaks of lava, low tremor activity showed fairly constant amplitude sustained for many days, or erratic showed fairly constant amplitude sustained for many days, or erratic fluctuations with peak amplitudes lasting from less than a minute to many minutes, or cyclic patterns with regular time intervals of amplitude changes. One variety of cyclic oscillation, descibed as gas piston activity (Swanson, 1971), was defined by tremor of low amplitude for 5-15 minutes during gradual rise of the lava column in the vent. The increased seismic signal during collapse of the lava column characteristically has a symmetrical cigar-shaped envelope: amplitude increases gradually,

reaches a peak at least several times above the initial background, and finally decreases at a rate comparable to the rate of increase during onset. Signal frequencies at peak amplitudes are 2-5 Hz at recording distance of about one kilometer from the eruptive vent. The tremor signal is generally local and decreases below background noise a few kilometers from the source vent. This oscillating pattern of lava and tremor activity, sometimes lasting for many days, was observed again during the Puu Oo eruption.
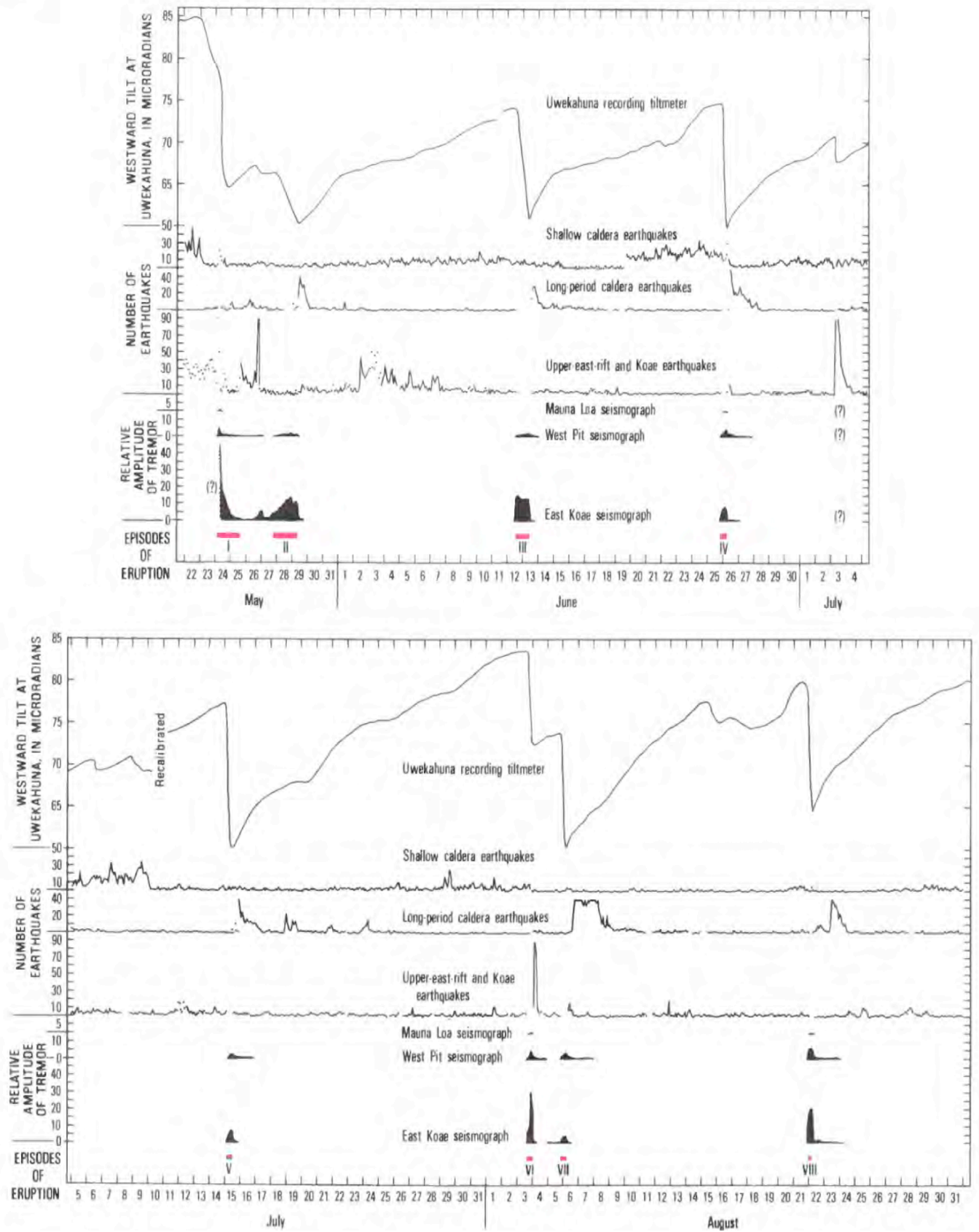
Fig.5. Plot of summit tilt, numbers of shallow earthquakes, relative amplitud of tremor and episodes of eruption for the Mauna Ulu eruption of Kilauea Volcano. May-October 1969. Tilt mesaurements

39

at 2-hours interval from the Uwekahuna east-west component tiltmeter near the northwest rim of Kilauea caldera. Earthquake counts at 2-hour intervals from selected local stations, detection threshold estimated at about magnitude 0.1. Amplitude of tremor taken from adjusted hourly readings of smoked-paper records and plotted in relative units above background noise at three stations: Mauna Loa (MLO), 25 km from the eruption site; West Pit (WPT), 11 km from the eruption site; and East Koar (EKO), 5 km from the eruption site. Times of major eruptive epsodes indicated by horizontal bars and labeled with their sequence numbers. Data beyond October incomplete and therefore omitted.
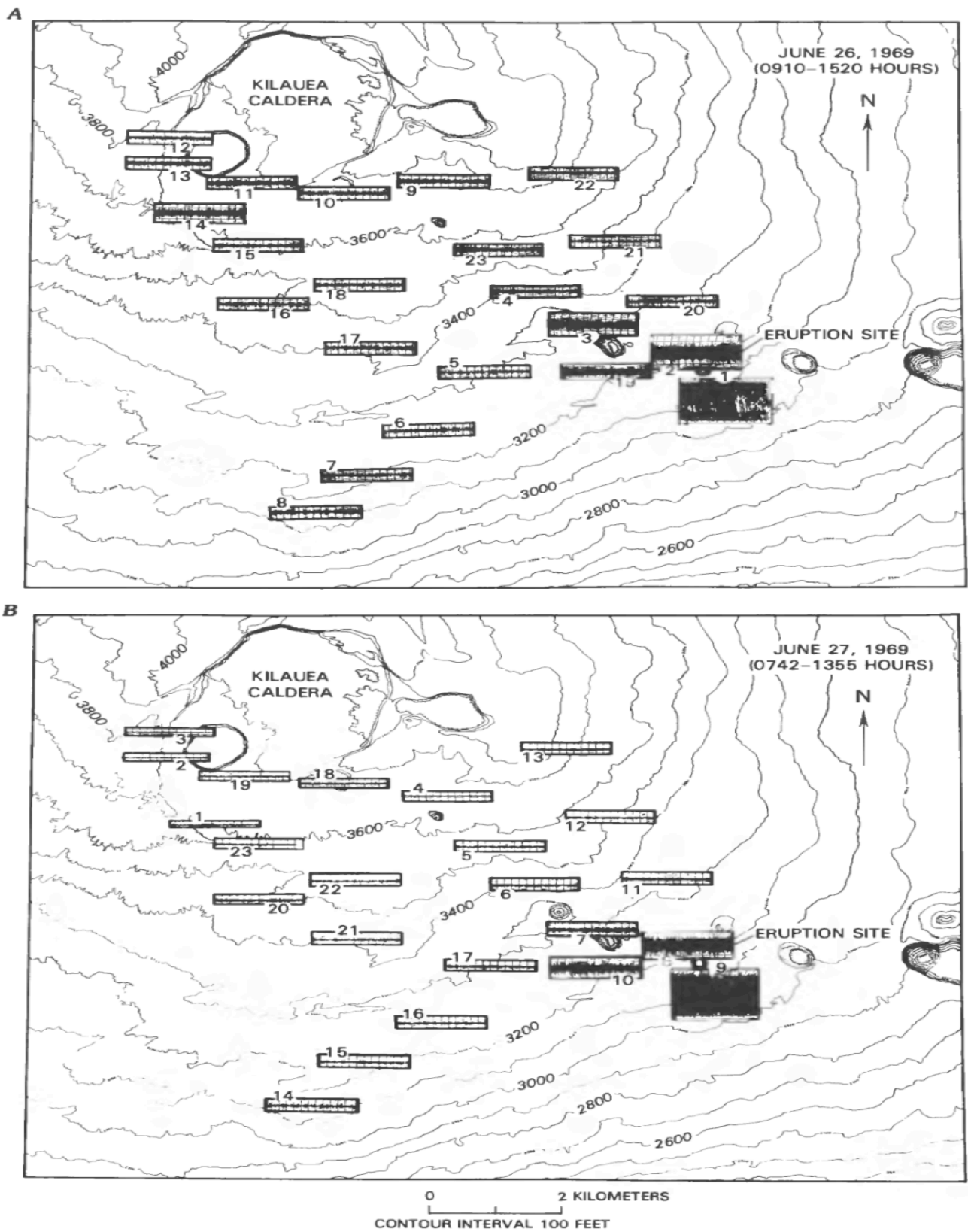
Fig. 6. Armonic tremor recorded by portable seismograph following eruptive episode IV of the Mauna Ulu eruption. The numbers indicate the order in which each site was monitored. All seismogram segments are one minute long . A, Immediatly after the eruptve episode. Note the

41

moderate-amplitude tremor at the summit stations 11 and 14. B, One day after the eruption. Note that tremor in the summit area (stations 1 and 19 here) has decreased to background noise.
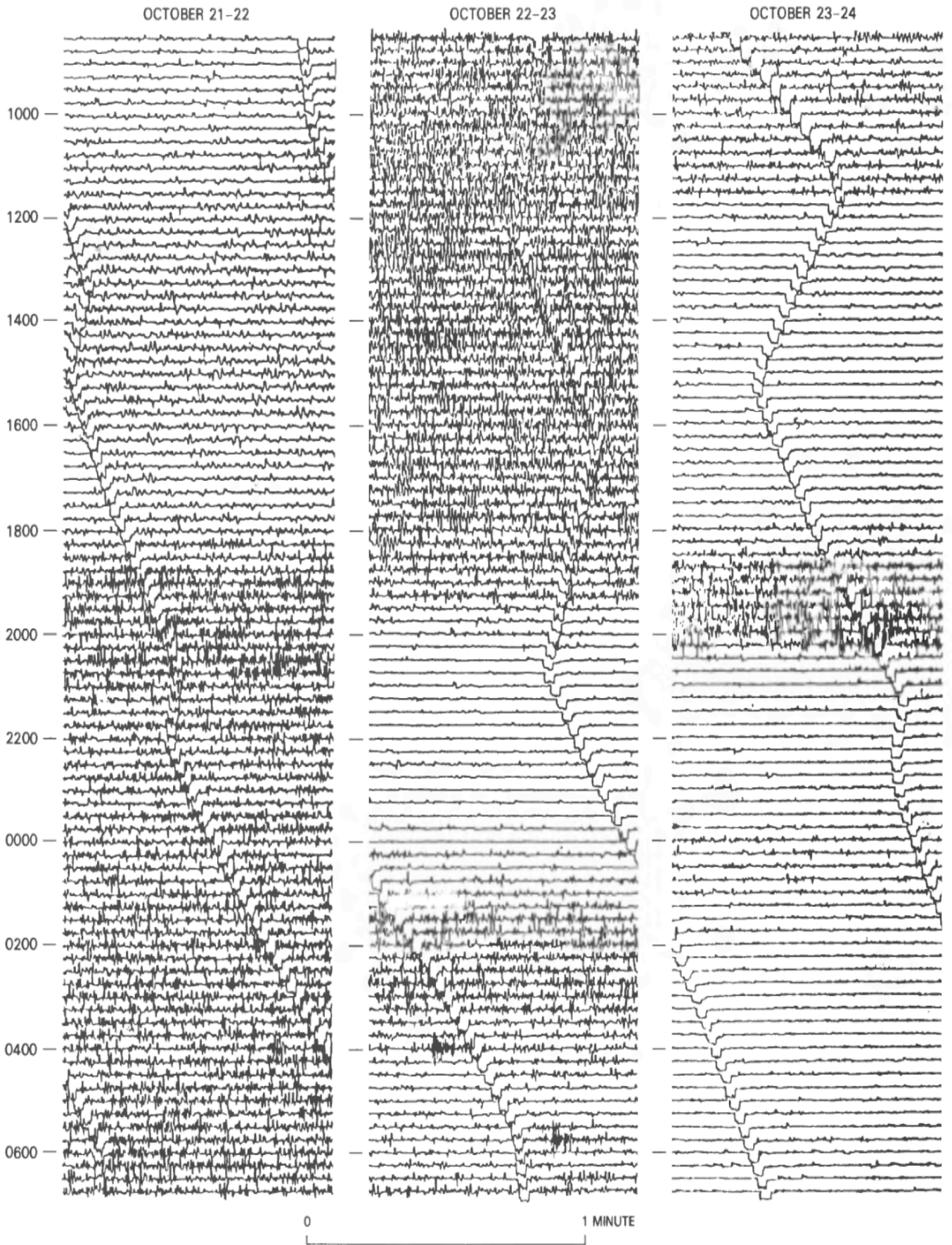
Fig. 7. Portions of a smoked-paper seismogram from station (EKO) on the upper east rift zone of Kilauea, 4.5 km from the eruptive vent, that monitored varying amplitudes of low tremor associated

with confined lava moment following a major episode of the Mauna Ulu eruption in October 1969. Recording speed and instrumental magnification were kept constant over the entire interval of time.

3.3 The Puu Oo eruption in 1983-1985

The pattern of seismicity from mid-1982 to 1985 and continuing reflects the mechanical process within Kilauea Volcano that developed into a major eruptive sequence in the east rift zone (Koyanagi and others, in pres). The geologic and geophysical data pertaining to the sequence of rift intrusions, fissure outbreaks, and eruptive episodes from a centralized vent system for this eruption from 1983 to mid-1984 are summarized by Wolfe and others. From Semptember to December 1982, increase of shallow earthquake in the summit region during periods of inflationary ground tilt, alternating with downrift-migrating swarms of earthquakes in the east rift zone during deflationary periods, indicated that episodic surges of magma were supplying the conduit sistem in the rift zone. This episodic activity led to a major intrusive event on January 2, 1983: rapid summit deflation and vigorous downrift migration of shallow earthquakes were sustained for 24 hours and finally resulted in a fissure outbreak in the east rift zone. High-frequency tremor accompanied the pre-eruption swarm of earthquakes in the east rift. The sustained deflation at the summit was accompanied by short-period earthquake, presumably due to fracturing of the host rocks in response to the withdrawal of magma, and harmonic tremor and long-period events associated with the accelerated magmatic activity. The onset of eruption was accompanied by a marked increase in east-rift tremor, followed by five days of incremental intrusion earthquakes and outbreak of lava farther downrift. The early weeks of the Puu Oo eruption were charavcterized by strong tremor with erratic high-frequency signals from a wide source area. As the pattern of eruption changed from fissure outbreaks to multiple –vent eruption and eventually to repeated lava emissions from e single vent system at Puu Oo, weaker and more continous harmonic tremor originated near the eruptive vent and corresponded in amplitude to the vigor of eruptive activity. Episodes of high lava fountains accompanied by high-amplitude tremor that usually lasted from less than a day to more than a week occurred at intervals of about one to nine weeks. Between major episodes of eruption, the

amplitude of the local tremor varied according to the level of the limited lava activity, which was sometimes visible, at depths of 0-50 m in the vent. The patterns of tremor recorded near the actice Puu Oo vent between eruptive episodes are illustrated in figure 8. As in the Mauna Ulu eruption, burst of moderate-amplitude tremor lasting about one minute occurred repeatedly during periods of low-amplitude tremor background tremor lasting 5-15 minutes that characterized gas piston activity (figure 8A). More sustained episodes consisting of increased amplitude lasting about three hours were observed during a repose period in February 1985 (figure 9B). major episodes of high fountains and lava output were accompanied by increased tremor, whose amplitude excceded by more than an order of magnitude de continuous backfround tremor during intervals of subdued eruptive activity. The rapid response of seismic amplitude to changes in lava fountaning and output rate imply that the principal source of tremori s shallow and localized at the eruption site. Convincing evidence of a deeper tremor source beneath the summit of Kilauea, separated from activity in the eruption region, was the tremor recorded at the North Pit following sustained high rates of deflactionary tilt at the summit. This relationship of tremor that varied in amplitude and duration according to the rate and magnitude of the episodes of the Puu Oo eruption from 1983 to mid-1984, and a reduction of the data indicating this relation is documented by Koyanagi and others. These episodes of summit tremor that accompanied major episodes of the eruption were frequently preceded by increasing rates ad amplitudes of discrete long-period events, which peaked into continuous tremor and then decayed gradually back to background, with bursts of long-period events, at progressively lower amplitude and wider intervals of time (figure 9). in contrast to both the summit storage zone and the east-rift eruption site, the rift conduit connecting them remained virtually free of detectable harmonic tremor during the repeated major episodes of eruption. From this we infer an absence of barriers in the central part of the lateral conduit system, allowing quasi-steady flow of magma with minimal pressure fluctuations. A chronological sequence of lava production, increased harmonic tremor in the east rift zone and

summit, and ground tilting is outlined in figure 10 for one of the vigorouse eruptive episodes in the prolonged east rift eruption. Ground tilt showing rapid deflation during the twenty-fifth eruptive episod in September 1984 (figure 10) was measured as the east-west component on a continuously recording tiltmeter located at Uwekahuna vault northwest of the summit deformation center. Deflationary tilt started gradually at about 1400 (H.s.t) on September 19 and accelerated in rate at 1700. It continued at a high rate until 0600 on September 20 and then gradually declined, ending by about 0900. The deflationary tilt during these 19 hours totaled 15 microradians, and it reached a maximum rate of 1.35 μrad per hour at about 2000 on september 19. Peak-to-peak amplitude of harmonic tremor was measured on Develocorder seismograms from station MPR for east-rift tremor and from station NPT for summit tremor. Ground oscillation in micrometers was reduced from the amplitude measurement averaged for about one minute at each hour and adjusted for instrumental magnification at the recorded frequency and for station corrections. The average period of the east-rift tremor signal recorded at MPR was about 0.5 s, and that of the summit tremor recorded at NPT was about 0.3 s. Station MPR, situated about 6 km west of the eruptive vent, recorded rapid increase and decrease of the east-rift tremor at the onset and end of the eruptive episode, with a temporary decrease in the middle. The hourly sampling rate used in figure 11 omitted a strong burst of tremor between 1622 and 1633 during the early activity, as well as the exact times of rapid changes at the onset and end of the vigorous fountaining episode.
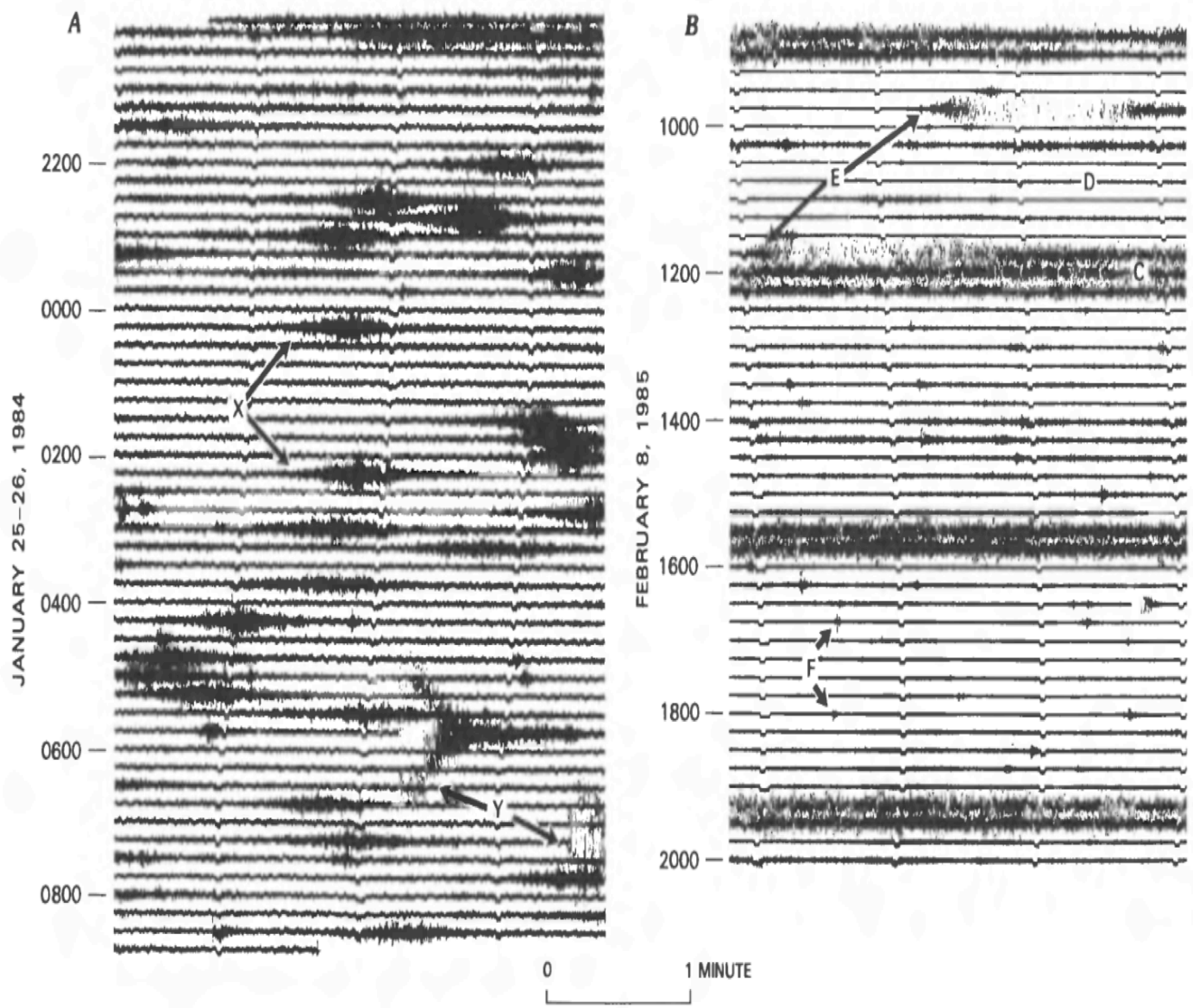
Fig.8. Portions of seismograms from revolving-drum recorders at stations on Kilauea Volcano showing various seismic events. A, Record from station PUK, about 1 km west of the eruptive vent Puu Ooshowing gas-piston events (X) and south flank earthquakes (Y). B, Record from station KMM showing a cyclic pattern of low tremor at the eruptive vent between the major episodes on February 4 and March 13, 1985, of the Kilauea east-rift eruption. Episodes of high tremor (C) less than an hour in duration repeatedly alternated with several hours of lower amplitude (D) during February 7-11, 1985. Two cigar-shaped (E) recorded at 0946 and 1145 were signals characteristic of cyclic lava movement, termed gas-piston acttivity, in the vent. Numerous microshocks (F) associated with thermal contraction crackingon the adjacent new lava flows, degassing explosions, and continual structural adjustments at the vent were conspicuous during times of lowbackground tremor. Other varieties of repose tremor during the prolonged eruption at Puu Oo are described by Wolfe and others.
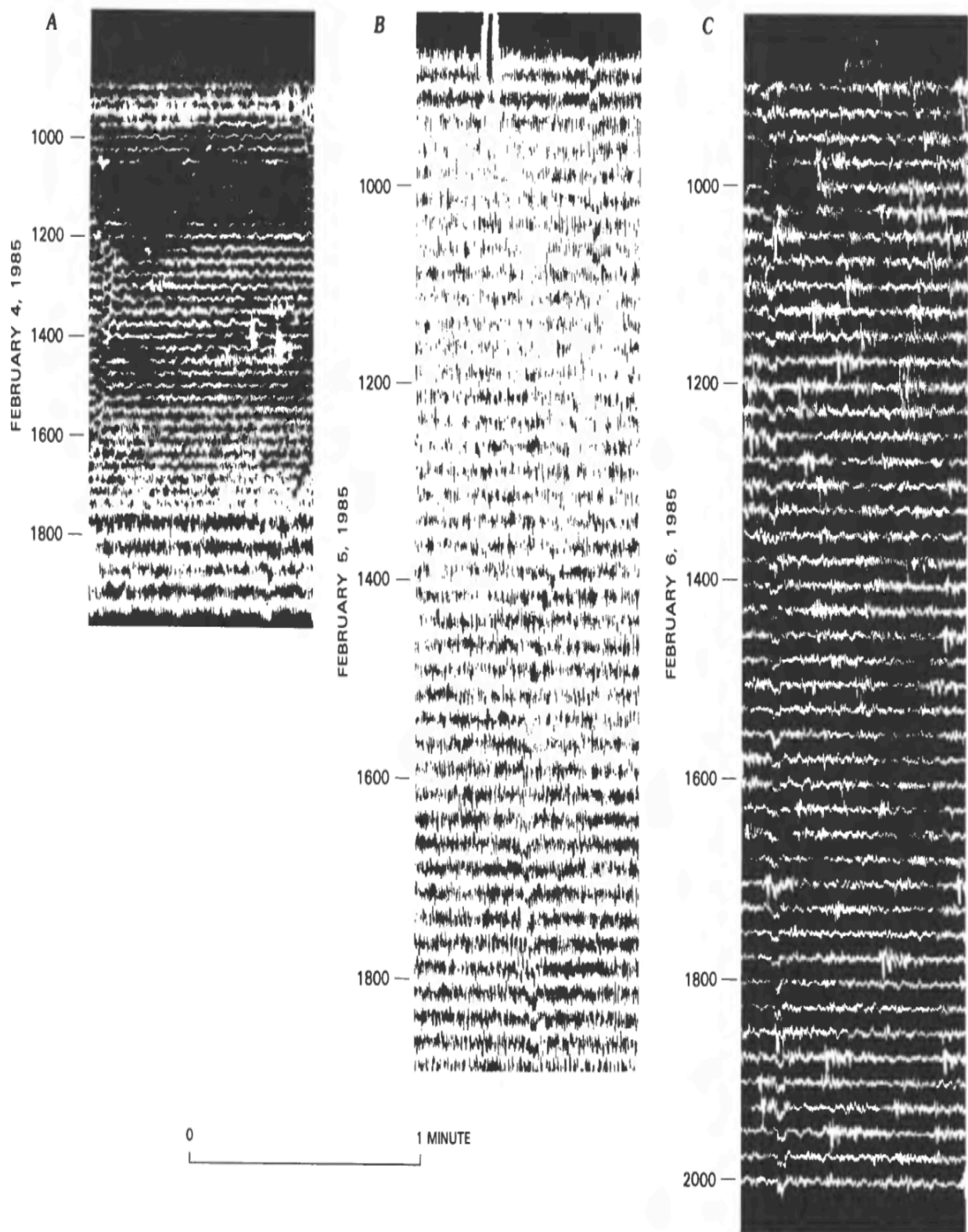
Fig.9. Section of smoked-paper seismograms from station NPT showing the sequence of harmonic tremor and long-period events at the summit following episode 30 of east-rift eruption on February 4-6, 1985. Recording speed and instrumental magnification were kept constant over the entire time interval. A, Period from 0900 to 2000 on February 6 shows an increased number of discrete long-period events in a decreasing background of continuous tremor. Occasionally, stronger long-period events were recorded widely on the summit network of station.
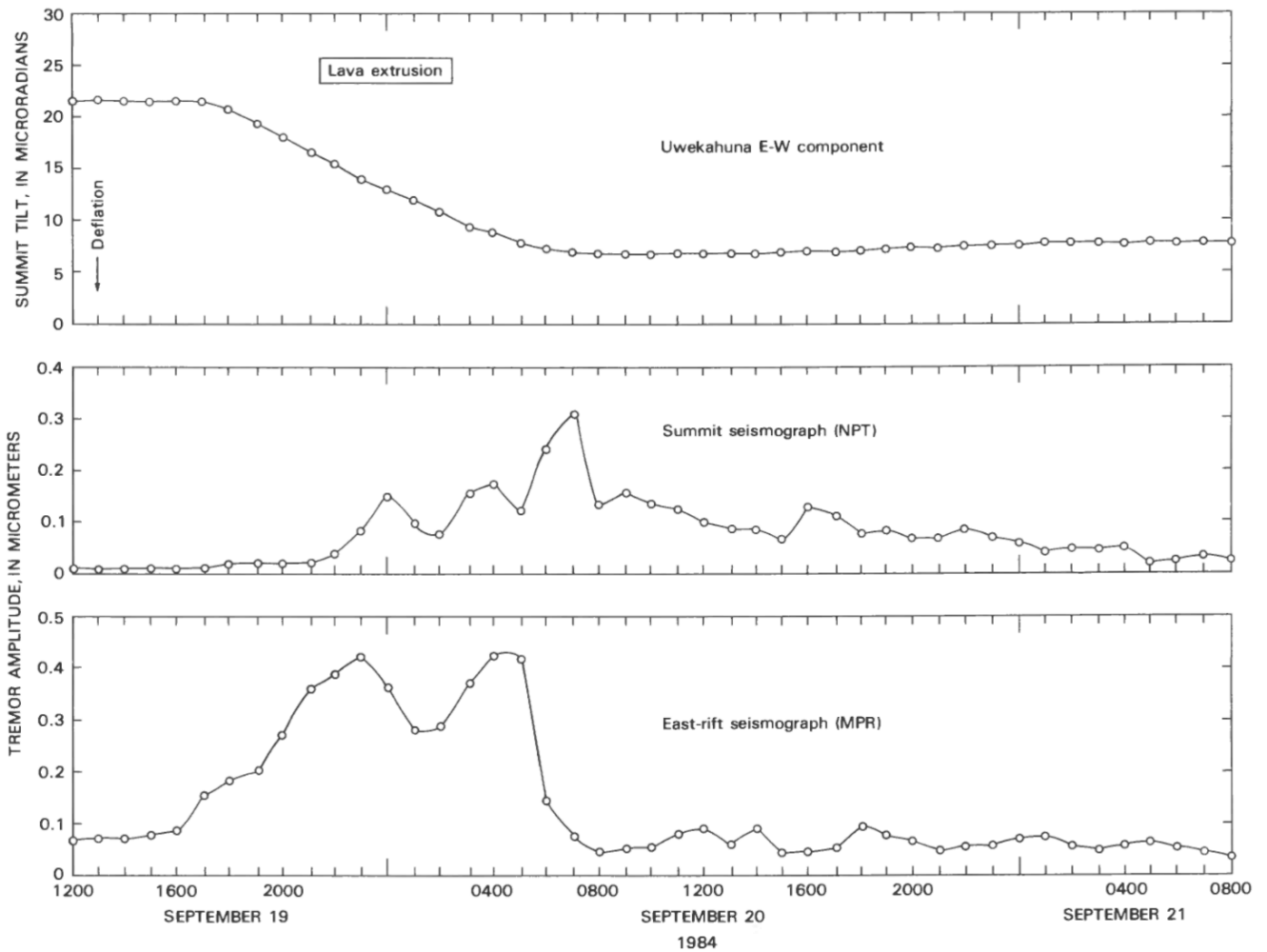
Fig.10. Change in tilt and tremor amplitude during and after episode 25 of the prolonged Kilauea east-rift eruption characterized by high lava production and fountaning. Tremor amlitudes are approximate averages, ±0.2 micrometers. Curves between hourly readings were interpolated.

2 Chapter

Methods of analysis applied to volcanic tremor

2.1 Method of spectral estimation

In most studies of volcanic tremor the estimation of the frequency content has been one of the primary tools for investigating the nature of the signal. However, any method used for the calculation of the spectrum should be able to cope successfully with a number of characteristics not present in other seismic signals. First, tremor can persist for long periods of time resulting in the accumulation of large amounts of data that have to be analysed. Second, they may exhibit strong temporal variations in amplitude and/or frequency content that should be monitored, because of their importance for source modelling and eruption forecasting. Third, the calculated spectrum may have multiple sharp peaks around narrow frequency bands, in which case a high degree of resolution is required in order to resolve the individual frequencies. One of the first spectral methods to be applied to digital tremor data was the direct segment method (Bath, 1974). The long tremor time series is divided into smaller non-overlapping segments and the spectrum is calculated for each segment by means of a Fast Fourier Transform (FFT). The final spectral estimate is then the average of all the individual spectra. This method has been used in volcanic tremor recordings from Mt. St. Helens (Fehler, 1983; Hofstetter and Malone, 1986). It enhances the spectral peaks that are common to every time segment and suppresses those generated by random

noise. A similar method for real-time spectral estimation of tremor data has been implemented at the Ruapehu volcano observatory (Hurst, 1985), where average spectra are calculated over successive 3-min intervals with a frequency resolution of 0.1 Hz in the band between 0.05 and 4.04 Hz (Sherburn et al., 1999) (Fig. 11). In order to detect temporal changes in the frequency content of the signal a direct comparison of the averaged spectra should be performed. Such a comparison of spectra from different time periods is feasible only when the amount of data is relatively small and the observed variations are larger than the ambient noise levels. A better way of detecting temporal variations is by incorporating in the display all the variables that are likely to change (time, frequency, amplitude). This accomplished by creating a spectrogram (Fig. 12), which is a 2D representation of the variations of spectral amplitude and frequency of the observed signal as time elapses. The calculation of the spectrogram can be achieved by moving a sliding window over the whole length of the time series and estimating the amplitude spectrum by performing an FFT for overlapping positions of the window (e.g. Mt. Semeru-Schlindwein et al., 1995; Ruapehu-Sherburn et al., 1999). The resolution of the spectrum obtained by using an FFT algorithm is proportional to the reciprocal of the window length chosen for the analysis. In order to increase the spectral resolution more than it is possible with the FFT, the Maximum Entropy Method (MEM) (Burg, 1967) has been applied in a number of cases (Pavlof- McNutt, 1986; Izu-Oshima-Yamaoka et al., 1991; Mt. Etna-Seidl et al., 1990). Assuming that the time series is generated by a linear random mechanism MEM fits to the data, in a least squares sense, an

autoregressive process of order p of the form (detailed derivations of these equations can be found in Ulrych and Bishop (1975)):

$$y_1 = \alpha_1 x_t + \alpha_2 x_{t-2} + \ldots + \alpha_p x_{t-p} + r_t \qquad (1)$$

by applying a prediction filter of length p, where α are the filter coefficients calculated by solving the normal equations posed by the least squares problem, r_t is a white noise series with zero mean and σ_α^2 variance. Then the spectrum of y_t will be estimated by the equation:

$$Y(\omega) = \frac{2\sigma_a^2}{|-\sum_{i=1}^{M} \alpha_i \exp(-i2\pi\omega j)|^2} \qquad (2)$$

where ω is frequency and M represents the total number of samples in the time series considered for the analysis. If the selected time window of the data is small enough MEM will produce a much higher resolution spectrum than the usual FFT methods, otherwise the result will be essentially the same.

2.1.2 Identification of source effects from observed spectra

Any recorded seismic signal can be considered as the result of the consecutive application of a series of linear filters to the original wavelet generated by a source (Lay and Wallace, 1995). This can be represented mathematically by the convolution of one filter with the other in the time domain :

$$W(t) = S(t) * P(t) * R(t) * I(t) \tag{3}$$

or the equivalent equation in the frequency domain:

$$W(\omega) = S(\omega)P(\omega)R(\omega)I(\omega) \tag{4}$$

where $W(t)$ is the recorded waveform, $S(t)$ is the original source wavelet, $P(t)$ represents the filter characteristics due to the propagation of the signal through the Earth, $R(t)$ represents filtering effects due to the structure beneath the recording station and $I(t)$ accounts for the filtering due to limited frequency bandwidth of the recording instrument. Hereafter we will refer to $S(t)$, $P(t)$ and $R(t)$ filters as "source", "path" and "site effects" respectively. Since in most cases the resulting spectrum consists of a series of sharp peaks, a major difficulty is to successfully determine which factors have shaped it. A comparison between tremor and earthquake spectra recorded at the same station is a common method of checking for possible site effects, since they should influence both signals (Mt. St. Helens-Fehler, 1983; Kilauea-Goldstein and Chouet, 1994; Deception Island-Almendros et al., 1997). Unfortunately it is far more difficult to find and isolate path effects, mainly because of the limited knowledge of the structure between the source and the receivers in most

volcanic areas. If the recording stations are close enough and azimuthally distributed around the source, similarities in spectra of different stations may be attributed to source effects (e.g. Pavlof-Mc Nutt, 1986). A less empirical approach to the source-path effect separation problem involves the use of spectral ratios for pairs of events recorded at a number of station (Sakurajima-Tsuraga et al., 1997). The method uses two time windows A and B from a tremor time series that were recorded at several different stations. Based on the assumption that these two events are generated by the same source and at the same hypocentral area, the path and site effects will be the same, thus Eq. 4 will be yielding spectral ratios of the storm $S^A(\omega)_i/S^B(\omega)_i$ for the ith station. The correlation of the estimated ratios for the all station and for different frequency bands can be checked by performing a statistical covariance analysis, where high correlation coefficients should indicate a common source effect for the two events. This method may not be always applicable, since the assumptions for events generated by the same source and at the same depth are not generally valid in every volcanic environment. The problem of the correct identification of specific frequencies as source effects and not as propagational artefacts has been made easier with the widespread use of spectrograms that display any new frequency as it appears. Since the path and site effect factors listed in Eq. 3 behave as linear filters and cannot generate new frequencies to their input signal (Anstey, 1981), these frequencies can only be attributed to a source effect.

2.1.3 Study of the wavefield properties – Polarisation analysis-

A further step in the analysis of the volcanic tremor is the study of its wavefield and the identification of the types of waves that compose it. The standard method that has been used for such an analysis is that of the covariance matrix (Montalbetti and Kanasewich, 1970; Jurkevics, 1988) which utilizes data recorded by one or more three-component seismometers. The method works in the time domain by badpass filtering the signal around the frequency band of interest and then calculating the covariance matrix for a short, sliding time window along the time series by using the following equation:

$$S_{ij} = \frac{XX^T}{N} = \frac{1}{N}\sum_{i=1}^{N} x_{ij}\, x_{ik} \qquad (5)$$

where $X = |x_{ij}|; i = 1,2,\dots,N; j = 1,2,2;$ is the data matrix in one window and x_{ij} is the ith sample of component j, N is the number of samples and T denotes the transpose of X. the estimated covariance matrix S will be of the form:

$$S = \begin{pmatrix} S_{zz} & S_{zn} & S_{ze} \\ S_{zn} & S_{nn} & S_{ne} \\ S_{ze} & S_{ne} & S_{ee} \end{pmatrix} \qquad (6)$$

where z, n, e denote the vertical, north-south and east-west components respectively and S_{ze} is the cross-variance of the vertical and east-west components, while S_{zz} is the auto-variance of the vertical component. Solving the eigenvalue problem $(S - \lambda^2)u = 0$ will give the three eigenvalues $(\lambda_1, \lambda_2, \lambda_3)$ and their corresponding eigenvectors (u_1, u_2, u_3). The three principal axes of the polarization ellipsoid will be given by $\lambda_j u_j$,

with $j = 1,2,3;$ the eigenvectors are equal to λ_j in amplitude units. One non-zero eigenvalue implies a purely rectilinear ground motion, while two non-zero eigenvalues characterize a purely elliptical palarisation. In order to obtain a measure of what kind of motion prevails in the time window the rectilinearity and planarity coefficients are used, that are given by $1 - (\lambda_2 - \lambda_3)/2\lambda_1$ and $1 - 2\lambda_3/(\lambda_1 + \lambda_2)$ respectively. The method described above has been used to study the wavefield properties of volcanic tremor from Mt. Etna for a time period spanning 6 years (1987-1993) during which different kinds of volcanic activity were at work, including periods of quiescence, Strombolian activity or lava fountaining (Ferrucci et al., 1990; Ereditato and Luongo, 1994; Wegler and Seidl, 1997). The polarization analysis for the whole of this period revealed a persistent pattern of high values for the rectilinearity coefficient with an east-west polarization, suggesting that the wavefield consists of waves radiated by a vertical extended source aligned along the north-south direction. The dominant wave types have been identified either as P waves (Ferrucci et al., 1990) or as Love/SH waves (Ereditato and Luongo, 1994; Wegler and Seidl, 1997) showing a complicated overlapping pattern. Similar observations have been reported for the tremor wavefield in other volcanoes, such as Arenal where the dominant wave type was identified as S waves by Benoit and McNutt (1997), whereas composition of the wavefield and were unable to identify any particular wave type.

2.1.4 Study of wavefield and source location using array methods
- Method of correlation coefficients –

While polarization analysis can give a qualitative picture of the composition of the tremor wavefield (even using data from only one seismometer), array methods can provide a much more detailed knowledge of it, at the expense of having to use more instruments and a specific receiver geometry. Aki (1957) designed and used the method of correlation coefficients in order to identify the predominant wave type of the background seismic noise generated by traffic in Tokyo. The method assumes that the recorded seismic signal is stationary and stochastic in time and space and that it consists mostly of surface waves, implying that the method can resolve wavefield properties generated by shallow sources. The spatial correlation function is calculated for pairs of receivers, one being at the centre of a semicircular array (reference receiver) and the others at its circumference, covering an azimuth of 0 to π degrees. This function is defined as:

$$\phi = (r, \varphi) = \langle u(x, y, t) \cdot u(x + r\cos\varphi, y + r\sin\varphi, t) \rangle \qquad (7)$$

where the angle brackets denote averaging over time, (x, y) and $(x + r\cos\varphi, y + r\sin\varphi)$ are the Cartesian coordinates of the two receivers, r is the distance between them and φ is the azimuth of the two receivers measured from the direction of the x axis. Integrating this function for the azimuth range covered by the array will give:

$$\phi(\bar{r}) = \frac{1}{\pi} \int_0^\pi \phi(r, \varphi) d\varphi \qquad (8)$$

For a wave with a phase velocity $c(\omega)$ the azimuthally averaged correlation function is related to the power spectrum $\phi(\omega)$ by the equation:

$$\phi(\bar{r}) = \frac{1}{\pi} \int_0^\pi \phi(\omega) J_0 \left[\frac{\omega}{c(\omega)} r \right] d\omega \tag{9}$$

where J_0 is the Bessel function of zero order. In almost all the cases one or more specific frequency bands are of interest: filtering the signal through a narrow bandpass filter centred at ω_0, the power spectrum will be $\Phi(\omega) = P(\omega_0)\delta(\omega - \omega_0)$, where $P(\omega_0)$ is the spectral power density of the signal at frequency (ω_0) and δ is the Dirac function. The correlation function will become:

$$\phi(\bar{r}, \omega_0) = \frac{1}{\pi} P(\omega_0) J_0 \left[\frac{\omega_0}{c(\omega_0)} r \right] \tag{10}$$

the correlation coefficient $p(r, \varphi, \omega_0)$ can then be defined as:

$$p(r, \varphi, \omega_0) = \frac{\phi(r, \varphi, \omega_0)}{\phi(0, \varphi \omega_0)} \tag{11}$$

and the azimuthal average of the correlation coefficients will be equal to:

$$\bar{p}(r, \omega_0) = J_0 \left[\frac{\omega_0}{c(\omega_0)} r \right] \tag{12}$$

it is possible therefore to calculate the correlation coefficients for different values of ω and azimuth φ, then fit a Bessel function to the coefficients and recover the phase velocity $c(\omega_0)$ of the recorded waves. By further analysis of the dispersion curves one may obtain the 2D velocity structure beneath the array for depths ranging 100 m to 1 Km. the equations that relate the correlation coefficients with the phase velocities of different wave types (Rayleigh, Love) can be found in Aki (1957, 1959). A contour map of the coefficients versus azimuth and frequency (Fig. 13) is used in order to determine the backazimuth of the incoming waves. Assuming that

a plane wave is propagating at a fixed azimuth θ, the correlation coefficients with the phase velocities of different wave types (Rayleigh, Love) can be found in Aki (1957, 1959). A contour map of the coefficients versus aximuth and frequency (Fig. 13) is used in order to determine the backazimuth of the incoming waves. Assuming that a plane wave is propagating at a fixed azimuth θ, the correlation coefficient will be:

$$p(r, \varphi, \omega_0) = \cos\left[\frac{\omega_0 r}{c(\omega_0)} \cos(\Theta - \varphi)\right] =$$
$$\cos[\omega_0 \tau(r, \varphi, \omega_0)] \tag{13}$$

where τ is the time delay between two receivers separated by distance r at an azimuth φ. In this sense ρ is costant along the wavefront $(\varphi = \theta \pm \pi/2)$ and decays in a direction perpendicular to it $(\varphi = \theta)$. Open conduit volcanoes that exhibit either permanent degassing or regular lava fountaining activity are good candidates for applying the correlation method, since the tremor source can be considered to a good approximation stationary and it is shallow enough to excite sufficient surface waves. The application of the method in three different volcanic systems (Kilauea-Ferrazzini et al., 1991; Masaya-Metaxian et., al 1997; Stromboli-Chouet et al ., 1998) showed that the recorded waves were coming from the summit crater of each volcano, where most of activity was visually observed. In the case of Masaya volcano, two arrays were available for the application of the method and the intersection of their backazimuth directions was used to lacate the tremor source. Although at Masaya and Stromboli the tremor wavefield was found to consist of both Rayleigh and Love waves, at Kilauea only Rayleigh waves could be identified after the study of their dispersion curves.

2.1.5 Semblance methods for source location

A realistic visualization of the tremor source should not only account for the temporal evolution of its properties, but should also extend spatially over some volume underneath a volcano, representing possibly a channel geometry over a magma reservoir or hydrothermal fluid circulation through a system of cracks. The methods discussed so far can pinpoint the area of origin of tremor, but cannot delineate in the three or even two dimensions. Furumoto et al. (1990,1992) attempeted to image the source of tremor at Izu-Oshima volcano using a portable array of vertical component seismometers. The array was situated near the crater and recorded tremor during a fissure formation episode. Their approach was to take advantage of the available multichannel data by calculating the semblance. (Neidel and Tanner, 1971) which is defined as:

$$S = \frac{\sum_{j=1}^{L} (\sum_{i=1}^{N} f_{i,j(t)})^2}{N \sum_{j=1}^{L} \sum_{i=1}^{N} f_{i,j(t)}^2} \tag{14}$$

Where N is the number of stations, $f_{i,j(t)}$ is a seismogram recorded at the ith station in the j time sampled and L is the number of samples that defines a time window. Assuming that the coherency of signal is being maximized in certain time windows because of phases arriving from a source, it is possible to calculate source-receiver travel time (Gottshammer and Surono 2000) applied a similar grid based method in order to locate the tremor source at Bromo volcano, but used signal power instead of semblance). In this way the spatial distribution of the semblance values can be depicted with the higher values covering the area of the seismic

source. In the case of Izu-Oshima only the high frequency (5-25 Hz) part of the recorded tremor was analysed using the method outlined above, because Furomoto et al. (1990, 1992) noted that inclusion of larger wavelengths would have resulted in the deterioration of spatial resolution due to the small aperture of the array (500m). The semblance distribution showed two separate areas with high values inside the caldera, which also coincided with the tips of the fissure that was formed during the eruption. Furumoto et al. (1992) suggest that these two source regions are the tips way up to the surface. The high frequency tremor was then interpreted as the result of the brittle fracture of rock owing to fluid-solid interaction as magma is being injected in the crack. An expanded definition of semblance has been used in order to locate the source region of volcanic tremor with a dominant period of 7-10 s (Mt. Etna-Seidl et al., 1981; Stromboli-Chouet et al., 1999; Mt. Aso-Kawakatsu et al., 1994, 2000; Mt Erebus-Rowe et al., 2000; Iwate –Nishimura et al., 2000). This kind of tremor appears in the time domain more as a swarm of discrete pulses rather than continuous episodes (Fig. 14); it occurs even when no signs of volcanic activity are observed and the particle motion indicates a high degree of rectilinearity with a direction pointing from each station to the crater of the volcano. In this case it is reasonable to assume that the source is isotropic and use the radial component ® from each station in order to calculate the semblance, penalising any departure from a pure rectilinear motion (caused by propagation effects) by subtracting the other components (V,T). The semblance will be:

$$S = \frac{\sum_{j=1}^{N}[(\sum_{i=1}^{N} R_{i,j(i)})^2 - N(\sum_{i=1}^{N} V_{i,j(i)}^2) - N(\sum_{i=1}^{N} T_{i,j(i)}^2)}{N \sum_{j=1}^{L} \sum_{i=1}^{N} R_{i,j(i)}^2} \qquad (15)$$

this definition takes advantage not only of a large number of stations that improve the signal to noise ratio, but it also incorporates independent information about the tremor wavefield, such as the rectilinearity. Kawakatsu et al. (2000) call this semblance "waveform semblance" and use it to locate the source region of the long-period tremor in a similar manner to that of Furumoto et al. (1990, 1992) (Fig. 15).

2.1.6 Visual and acoustic observations related to tremor activity

An important way of gaining insight into the physical processes that generate tremor and other volcanoseismic phenomena is the visual monitoring of the eruptive activity. Even though a range of different factors may be involved when it comes to a decision for conducting such observations (accessibility to the erupting site, possible danger posed to the lives of the scientific crew, use of different type of instruments like video camera, etc.) the independent information that will be collected may play a significant role for explaining possible physical mechanisms. Detailed visual observations described by Ferrazzini and Aki (1992) during a seismic experiment at Kilauea combined with instrument recordings enable them to distinguish between the different physical mechanisms that generate tremor and spindle-shaped signals called gas-piston events (Swanson et al., 1979). High-amplitude tremor was being recorded during the first month of the experiment and visual observations around the crater indicated lava fountaining activity while glows could be seen at night. A decrease in the tremor amplitude marked the onset of gas-piston events reflecting a change in the volcanic activity: the level og the lava lake in the crater started rising, with upwelling domes appearing at the surface of the lake and bursting of bubbles started occurring. After that the level of the lake fell, but the same kind of ponding and withdrawal of lava continued in episodic cycles. Tremor signals accompanied by sounds observed in volcanoes that exhibit explosive degassing activity (Fig.16)

prompted researchers to the investigate the possibility of a common link between the two phenomena. Even though it has been well know that volcanic eruptions can generate pressure disturbances in the atmosphere with a frequency that can range between 10^{-3} and 20 Hz (Richards, 1963), until recently there was no systematic recording of the temporal variations of these signals near erupting volcanoes. Nowadays the installation of very sensitive microphones that record air-pressure waves with high resolution is an important supplement to the seismic monitoring of active volcanoes (Stromboli-Ripepe et al., 1996; Pavlof-Garcés and Hansen, 1998; Arenal-Garcés et al., 1998; Sakurajima-Garcés et al., 1999; Karimsky/Sangay-Johnson and Lees, 2000; Mt. Erebus-Rowe et al., 2000) in the case of the Pavlof 1996 eruption, a common pattern of signals was observed consisting of pairs of short duration low-frequency/high-frequency phases on the seismograms superposed on the background tremor (Fig. 17) while at the same time explosion sounds were recorded by the microphones. An explanation for the appearance of these two phases during explosion episodes has been given by Garcés and Hansen (1998) based on the concept of a stratified magma column. This column is assumed to be composed of layers of magma with depth- and time-varying physical properties. While the deepest parts are dense and viscous, exhibiting high sound velocity, the shallower layers become less dense because of increase in the bubble content owing to degassing that lowers their sound velocity. A steady flow of magma from a deeper reservoir is not expected to alter the stratification, therefore the deepest, dense layer acts as the area of generation of seismic waves (tremor) that, due to the sharp impedance contrast with the upper parts, can only propagate in the surrounding

bedrock (low-frequency part). A similar process may occur in the shallower layer where metastable gas mixtures of H_2O and CO_2 can produce explosions that can only propagate in the atmosphere and then back to the ground (high-frequency air wave). On the other hand, an unstable, turbulent flow of magma can disrupt the stratification and smooth the density contrast between the layer boundaries so that it is possible to have sound waves propagating through the different parts of the magma column. Theoretical models of these processes have been published by Garcés (1997) and Garcés and McNutt (1997), while results from their direct application to model waveforms of seismoacoustic data acquired during the 1996 eruption of Pavlof volcano have been published by Garcés et al. (2000). Table 1 summaries visual as well as acoustic observations related to tremor activity reported at volcanoes around the world.
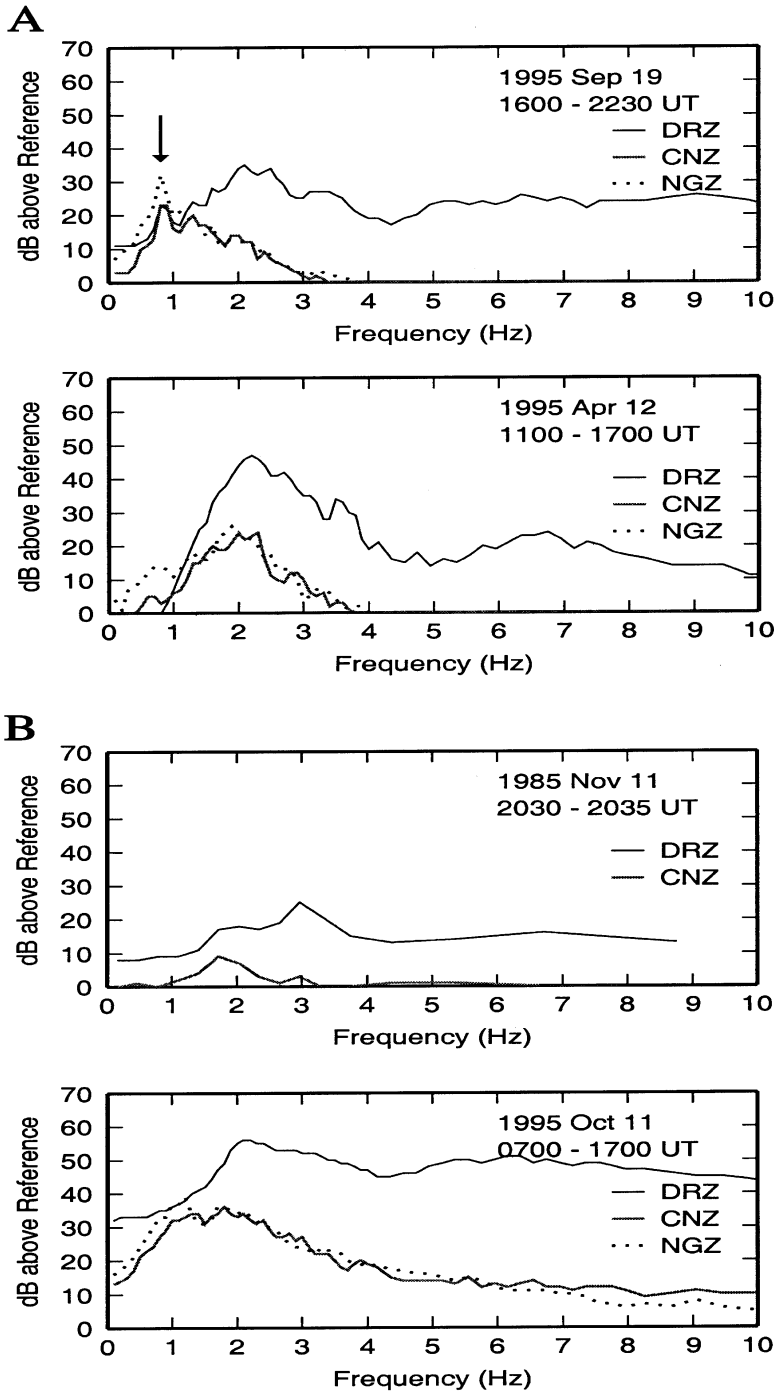
Fig. 11. (A) Amplitude spectra of tremor from Ruapehu showing a peak at 0.8 Hz (marked with arrow) and peaks at 2 and 7 Hz. The spectra are an average of 129 3-min readings over a period of 6.5 h from three different stations (after Sherburn et al., 1999). (B) Same as in (A) for tremor with peaks at 2 and 3 Hz and wideband tremor (after Sherburn et al., 1999).
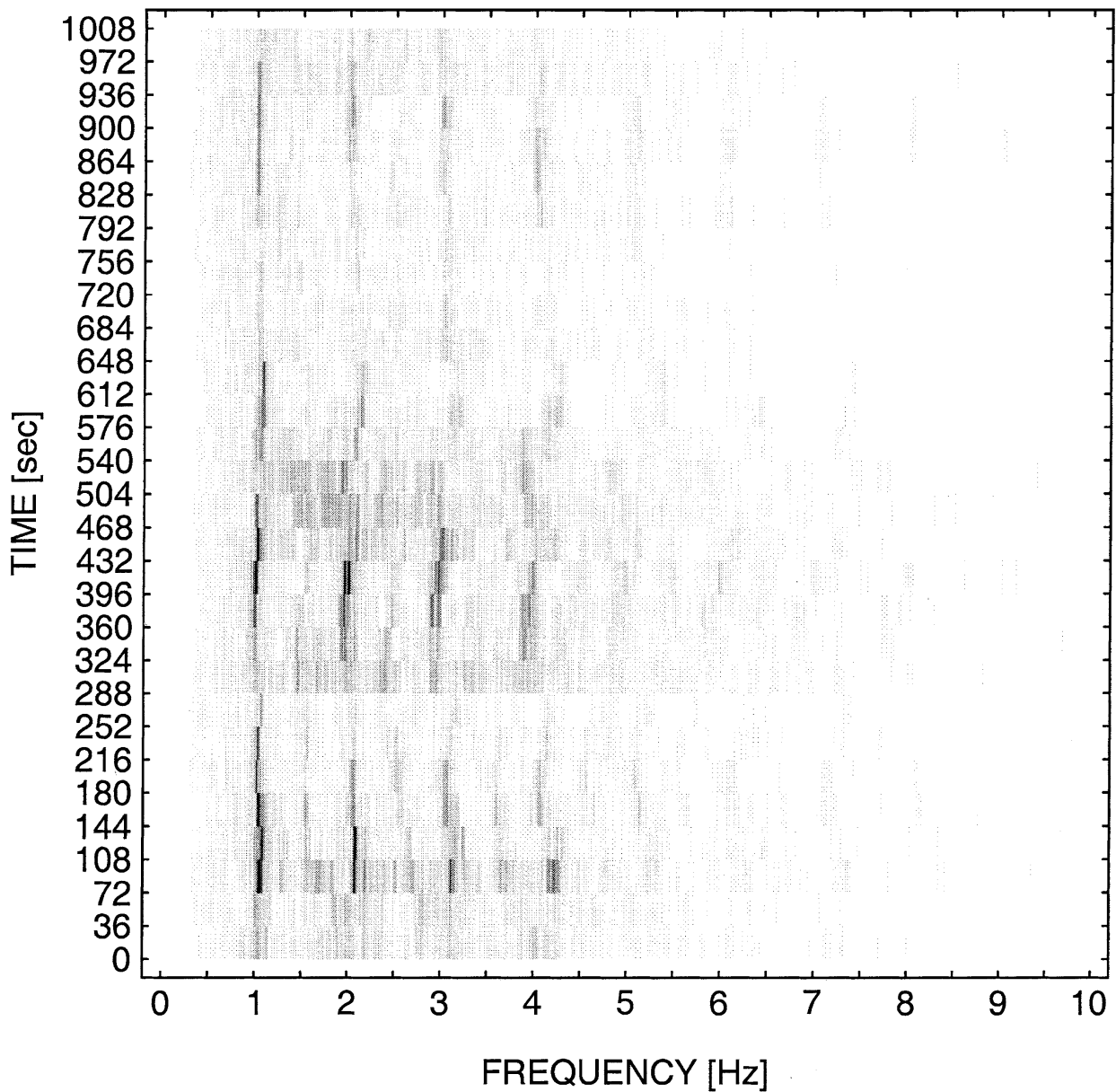
Fig. 12. spectrogram of tremor recorded at Mt. Semeru with 10 harmonics clearly visible. The vertical axis mark the beginning of every calculation window and dark shades indicate high energy, light shades low energy. Note how the spectral lines representing each harmonic shift as time elapses, keeping the same horizontal distance from each other; this phenomenon , which has been termed "gliding", was also observed at Arenal volcano by Hagerty et al. (2000) (from Schlindwein et al., 1995).
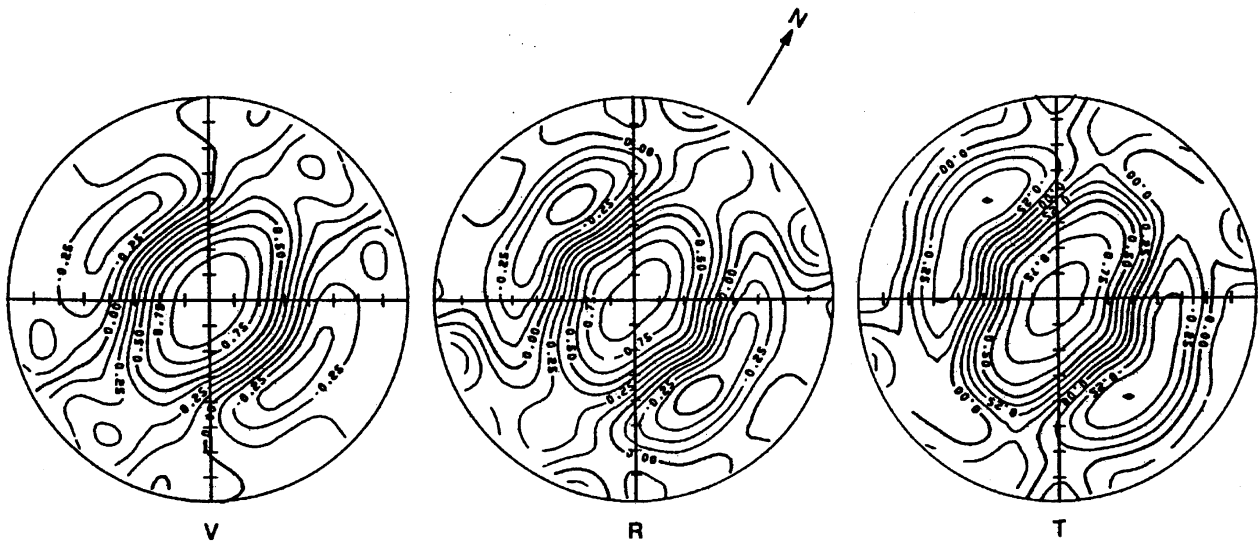
Fig. 13. Contour maps of the correlation coefficients $\rho(r, \varphi, \omega_0)$ calculated from tremor data recorded at Kilauea (Pu'u O'o crater) over a window of 180 s. the three plots correspond from left to right to the vertical, radial and transverse component. The frequency axis is taken along the radius of the circle with the origin at the centre. Note the rapid decrease of values along the EW direction, while they remain almost constant along the NS which is the direction that the wavefront is oriented (from Ferrazzini et al., 1991).
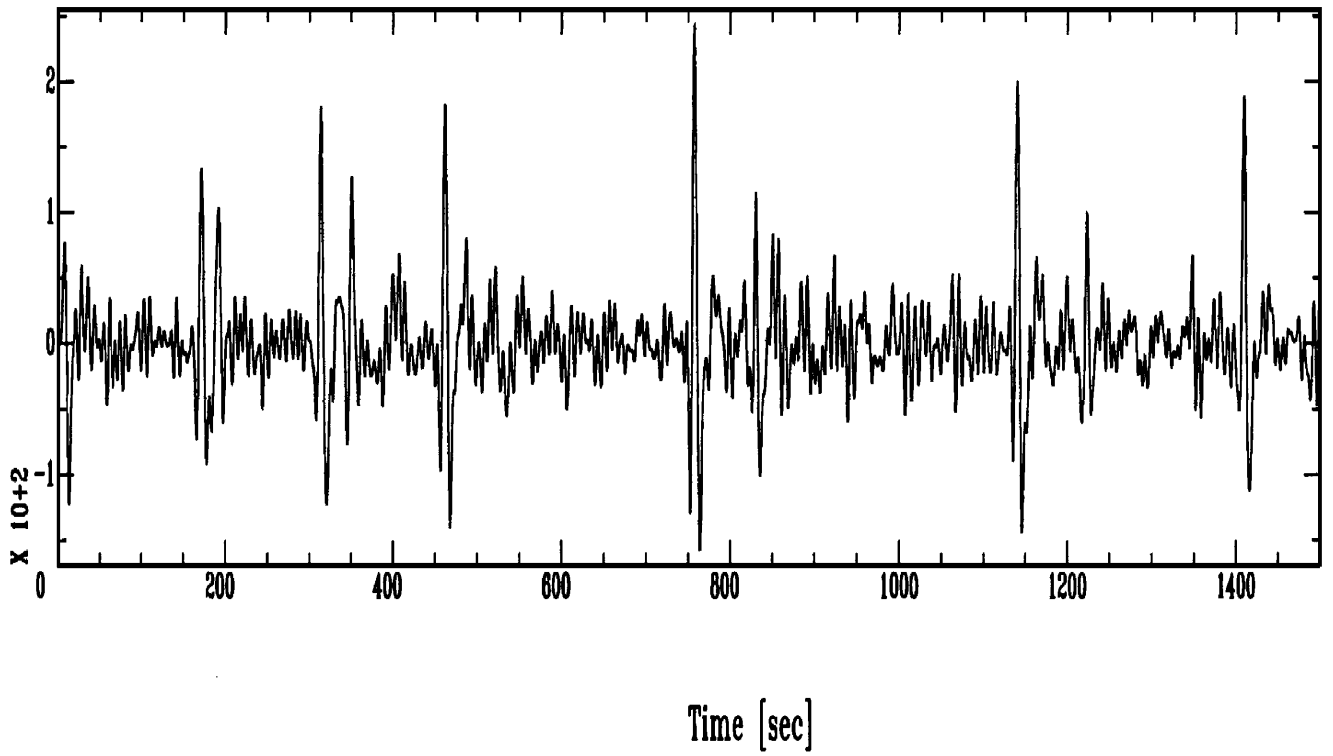
Fig. 14. Vertical velocity waveform of very long period tremor recorded at Pu'O'o crater Hawaii. The trace has been bandpass filtered between 0.01 and 0.1 Hz (from Bond, 2000).
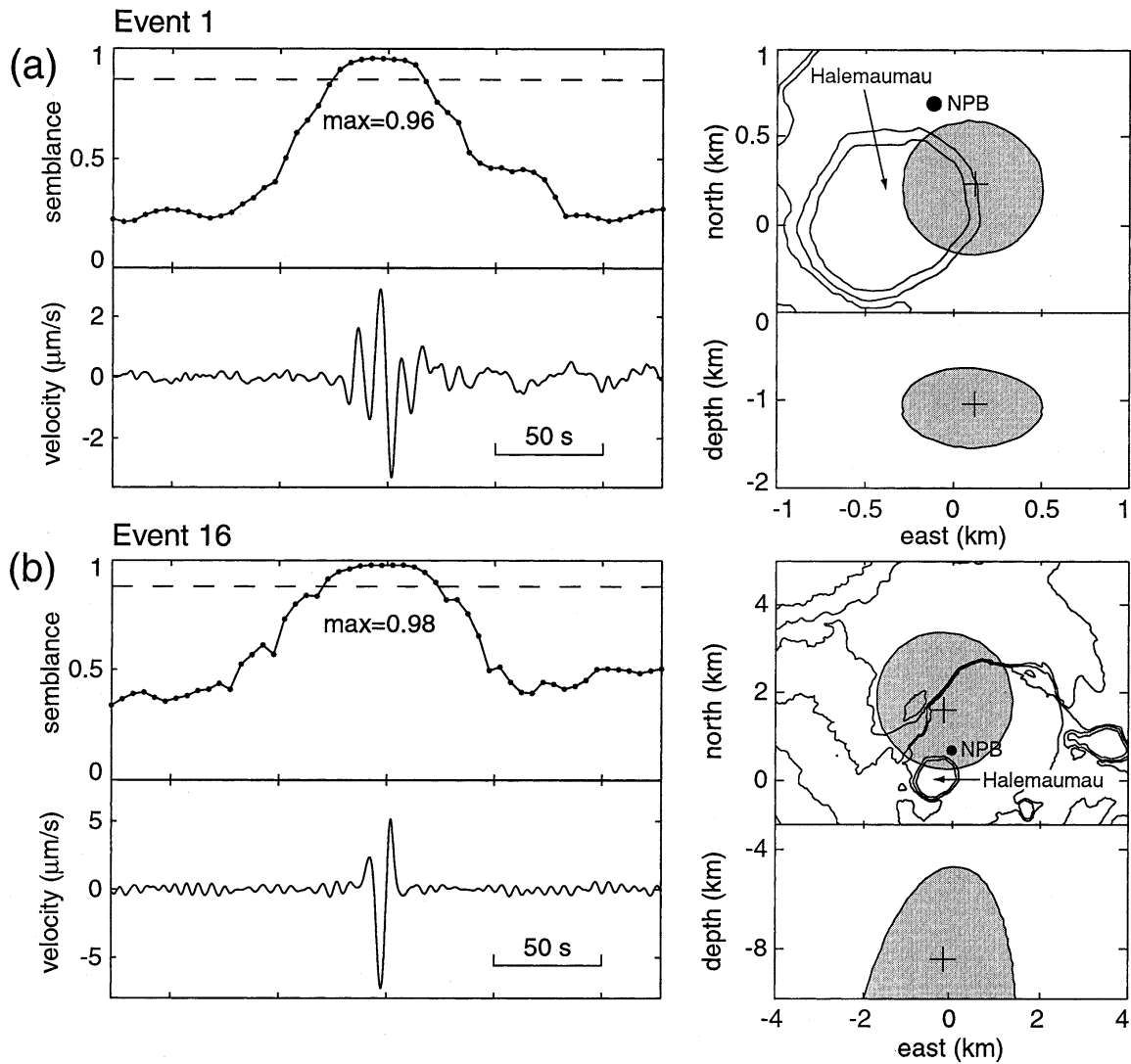
Fig. 15. Example of location of two very long-period tremor events using the waveform semblance method, from Pu'u O'o crater, Hawaii. The source position in the maps and the depth cross-section on the right is represented by a cross, whie the shaded area shows the size of the error region (from Almendros et al., 2002).
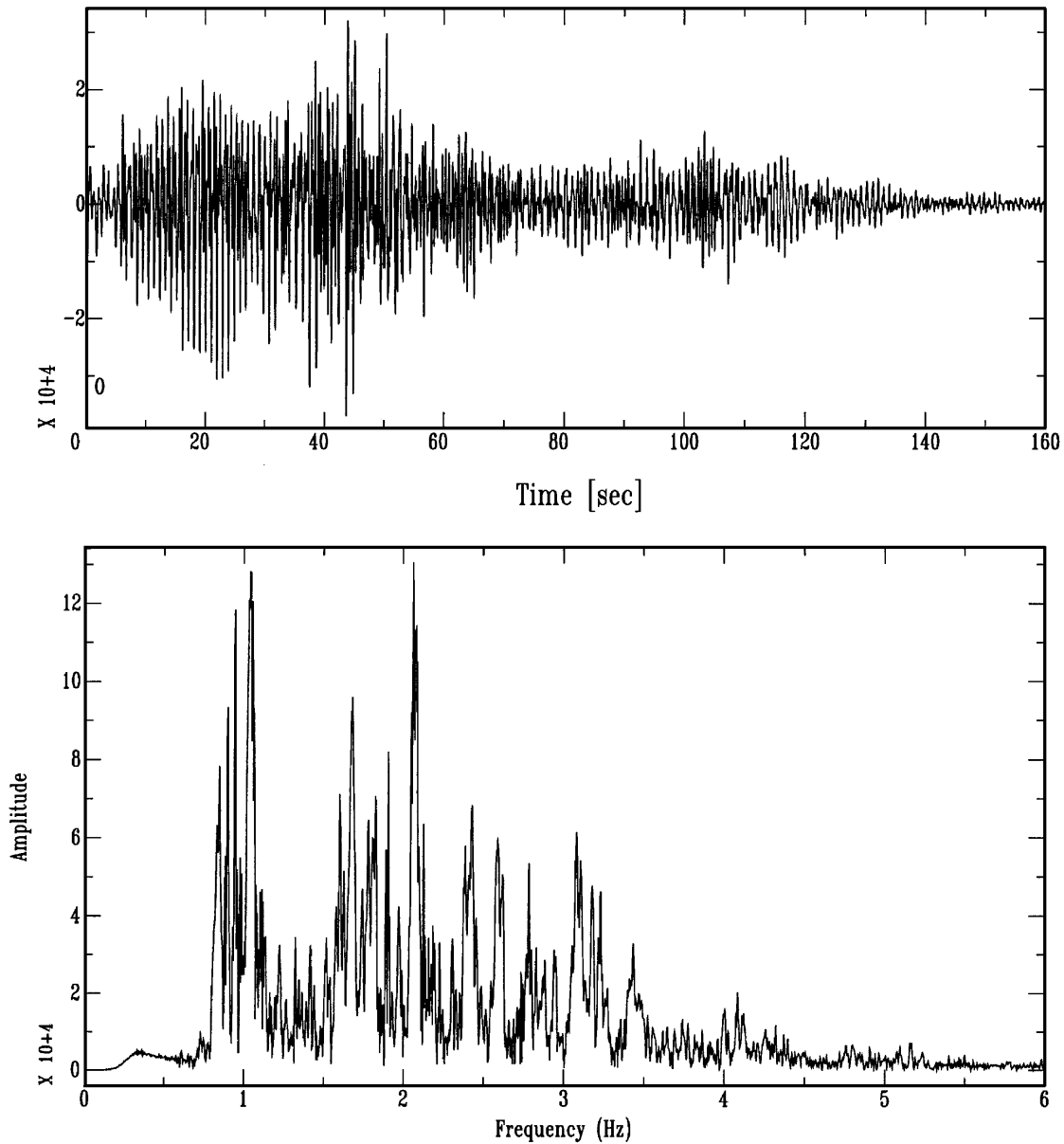
Fig. 16. Vertical component velocity waveform (bandpass filtered 0.3-10 Hz)and amplitude spectrum of a tremor episode recorded at Sangay volcano, Ecuador. This kind of quasi-periodic tremor has been termed a "chugging" event and is commonly accompanied by a sound resembling that of a steam locomotive. Similar events to this have been also observed at Arenal volcano, Costa Rica by Benoit and McNutt (1997).
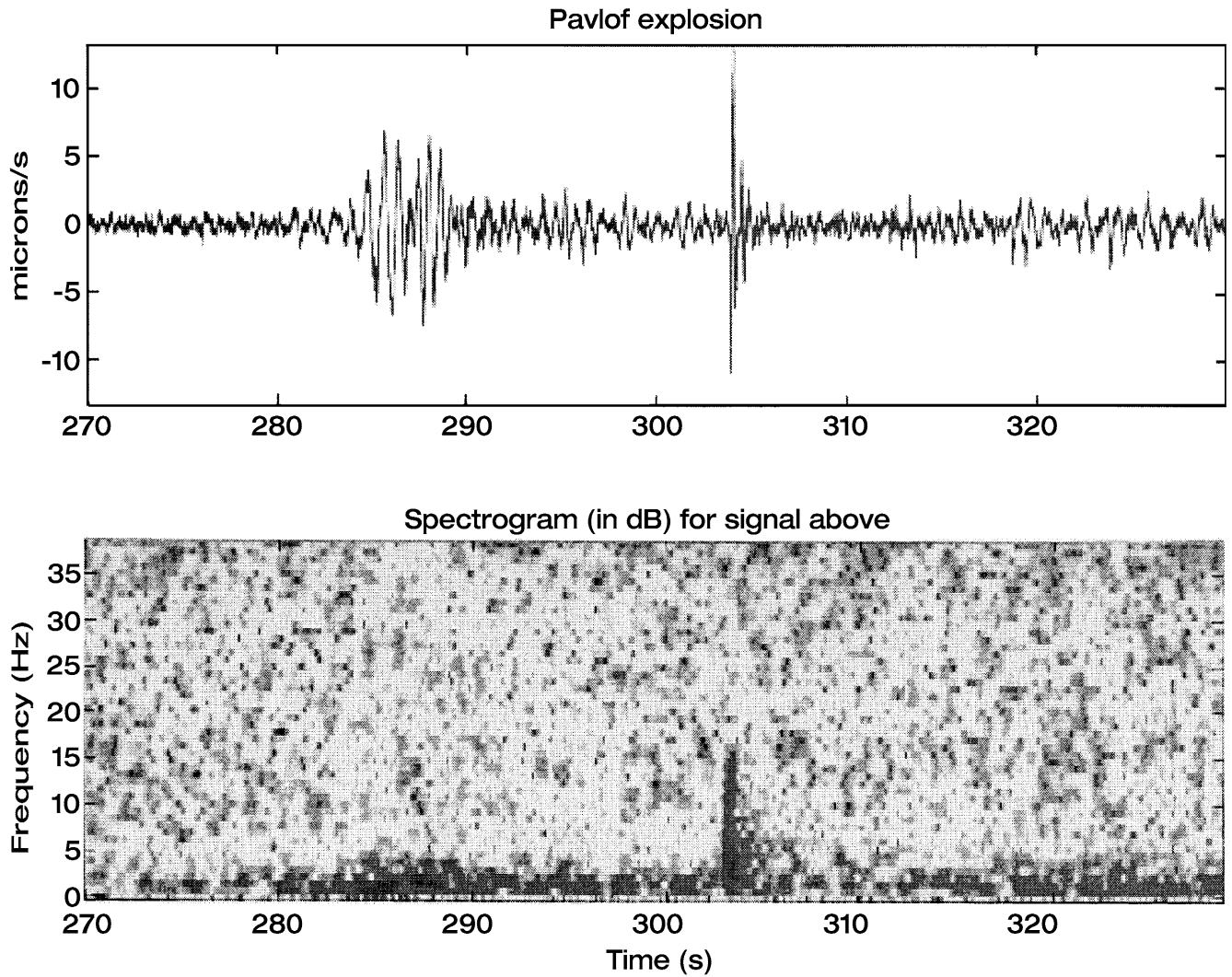
Fig. 17. Velocity waveform and spectrogram of an explosion signal with a low-frequency/high-frequency pair superposed on the background tremor, recorded during the 1996 eruption of Pavlof. The spectrogram was calculated using a sliding 1.28-s Hanning window with 90% overlap. Dark shades indicate high energy and light shades low energy (from Garcés and Hansen, 1998).

Reported visual and acoustic observations related to tremor activity

Region	Visual/acoustic observation	Reference
Pavlof	Lava fountaining related to high-amplitude tremor	McNutt, 1986; Garcés and Hansen, 1998
Klyutchevskoy	Variation of tremor spectral amplitude envelope whenever the eruptive activity changed	Gordeev et al., 1990
Kilauea	Gas-piston events associated with cycles of ponding and withdrawal of lava from the crater followed by high-amplitude tremor	Ferrazzini and Aki, 1992
Mt. Semeru	Pumping and explosion sounds with durations of 40 s–16 min that coincided with tremor episodes	Schlindwein, 1994
Stromboli	Gas bursts at the top of the magma column coincide with high-amplitude tremor	Ripepe et al., 1996; Ripepe, 1996
Arenal	Different explosion sounds that are accompanied by ash plumes and precede tremor episodes	Benoit and McNutt, 1997; Garcés et al., 1998; Hagerty et al., 2000
White Island	Eruptive/intrusive activity always followed by inharmonic tremor	Sherburn et al., 1998
Satsuma-Iwojima	Strong tremor occurring while vent emmits high-temperature volcanic gas	Ohminato and Ereditato, 1998
Karimsky/Sangay	'Chugging' tremor episodes followed by steam locomotive-like sounds	Johnson and Lees, 2000

2.1.7 Volcanic tremor at Stromboli

Stromboli volcano is in a steady explosive state with volcanic tremor as stationary phenomenon. It has been demonstrated that at Stromboli volcanic tremor assumes different amplitudes according to different explosive activity of the volcano. High explosivity generally coincides with an increase of the volcanic tremor amplitudes (Nappi, 1976) while during period with few explosions, volcanic tremor shows low amplitudes. Source models have to deal with the low frequency range of the seismic signal (from 1 to 5 Hz) and stability of some spectral peaks. Physical models proposed to explain the origin volcanic tremor take into consideration resonant effects produced by the geometry of volcanic conduits or by vibrations of a fluid filled tensile-crack generated by an excess of pressure in the fluid magma. Tremor could be originated from resonant effects produced by the geometry of volcanic conduits (Seidl et al., 1981; Ferrick et al, 1982). According to this model, different frequency content of the seismic signal is directly linked to the length of the conduit sections. A different model suggestes that volcanic tremor is produced by vibrations of a fluid-filled tensile-crack (Aki et al., 1977). Vibrations would be generated by an excess of pressure in the fluid. Magma, moving through sudden openings of tiny cracks, produces tremor. Following this model, it has been proposed (Chouet, 1985) that fluid magma vibrates according to oscillations of the crack. In spite of the different dynamics proposed to explain the origin of volcanic tremor, there is general agreement on the fundamental role played by pressure fluctuations in magma dynamics to generate seismic signals (Ripepe, 1995). Since 1993

the use of high sensitive pressure sensors in very near field conditions (150 m from the vent) at Stromboli has revealed that small gas bursts, which are not producing clear seismic transient signals, generate low pressure impulses. According to simultaneous infrasonic and seismic records, we suggest that volcanic tremor at Stromboli is produced by the pressure drop arising from the explosions of small gas bubbles, once they reach the top of the magmatic column. In a volcanic systems with open conduits, the explosive source can be thought to be confined at the top of the magmatic column. In this case the source is represented by exploding gas pockets contained in the fluid magma. This is confirmed by experiments of simultaneous records of seismic and air waves produced by the same volcanic explosion (Braun and Ripepe, 1993). Frequency contents (3-8 Hz), propagation velocity (340 m/s typical of sound speed in the air at 300 K) and low pressure values (5-8 Pa), measured at a distance of 150 m from the crater, bring to the conclusion that these atmospheric pressure waves, correlated to volcanic explosions, are infrasonic (Vergniolle and Brandeis, 1994). The high sensitivity and the small distance (150m) from the vent of the pressure sensors used, have revealed unusual infrasonic signals even in absence of volcanic explosions. The striking relationship between energy variation of infrasonic impulses and seismic energy fluctuations indicates that infrasonic and volcanic tremor are linked together to a common source. This source is dynamically represented by the burst of small gas bubbles at the top of magmatic column.

3 Chapter

Finite element method.

3.1 The physical domain.

The first thing we have to describe is the geometry (Figure 1). we are thus given a polygon in the plane $\mathbb{R}^2$. We call this polygon Ω. Its boundary is a closed polygonal curve Γ. The boundary of the polygon, Γ, is divided into two parts, that over the whole of Γ and do not overlap:
- The Dirichlet boundary Γ_D,
- The Neumann boundary Γ_N.

The Dirichelt boundary is where diaplacements are given as data; the Neumann boundary is where normal stresses are given as data. Each of these two parts is composed by full sides of the polygon.
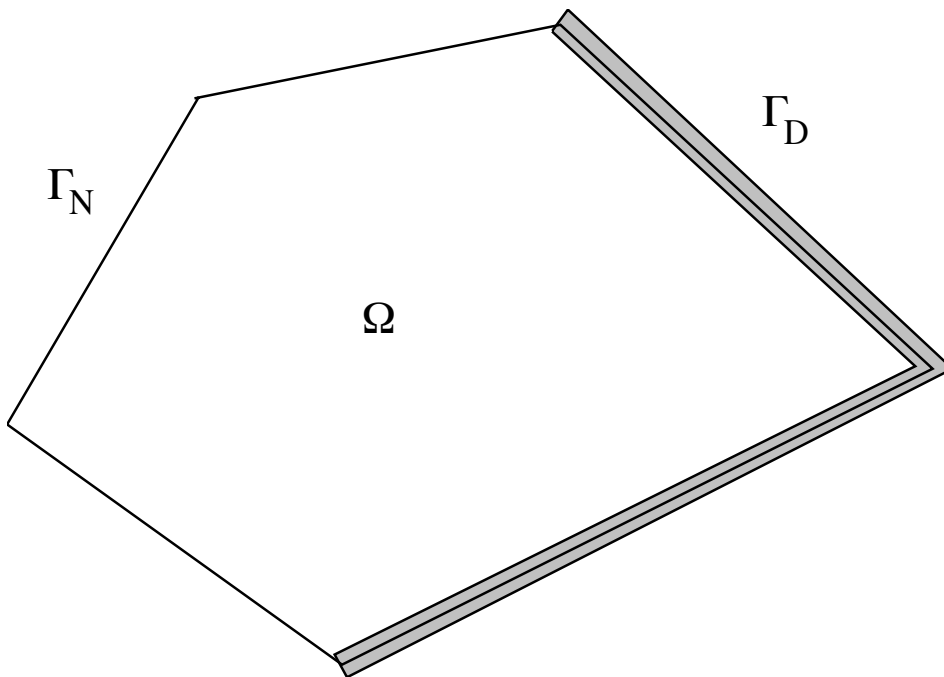

Figure 1: The domain Ω and the Dieichlet and Neumann boundaries.

3.2 Green's Theorem

The approach to solve this problema bove with the Finite Element Method is based upon writing it in a completely different form, which is sometimes called weak or **variational form**. The most important theorem in this process or reformulating the problemi is Green's Theorem, one the most popular results of Vector Calculus. Sometimes it i salso called Green's First Formula. The theorem states that

$$\int_\Omega (\Delta u) + \int_\Omega \Delta u \cdot \Delta u = \int_\Gamma (\partial_n u) v$$

note that there are two types of integrals in this formula. Both integrals in the left-hand side are domain integrals in Ω, whereas the integral in the right-hand side is a line integral on the boundary Γ. The resulti s also true in three dimensions. In that case, domain integrals are volume integrals and boundary integrals are surface integrals. The dot between the gradients denotes simply the Euclidean product of vectors, so

$$\Delta u \cdot \Delta v = \frac{\partial u}{\partial_{x1}} \frac{\partial v}{\partial_{x1}} + \frac{\partial u}{\partial_{x2}} \frac{\partial v}{\partial_{x2}}$$

3.3 The problem, written in weak form

The departure point for the weak or variational formulation is Green's Theorem. Here it is again

$$\int_\Omega (\Delta u) + \int_\Omega \Delta u \cdot \Delta u = \int_\Gamma (\partial_n u)v = \int_{\Gamma_D} (\partial_n)v + \int_{\Gamma_N} (\partial_n)v.$$

Note that we have parted the integral on Γ as the sum of the integral over the two sub-boundaries, the Dirichlet and the Neumann boundary. Now we substitute what we know in this formula: we know that $\Delta u = f - cu$ in Ω and that $\partial_n u = g_1$ on Γ_N. Therefore, after some recording

$$\int_\Omega \nabla u \cdot \nabla v + c \int_\Omega uv = \int_\Omega fv + \int_{\Gamma_N} g_1 v + \int_{\Gamma_D} (\partial_n u)v$$

Note now that we have written all occurences of u on the left hand side of the equation except for one we have left on the right. In fact we don't know the value of $\partial_n u$ on that part of the boundary.

$$v = 0, \qquad \text{on } \Gamma_D$$

therefore

$$\int_\Omega \nabla u \cdot \nabla v + c \int_\Omega uv = \int_\Omega fv + \int_{\Gamma_N} g_1 v \text{ if } v = 0 \text{ on } \Gamma_D$$

We have not imposed yet the Dirichlet boundary condition ($u = g_0$ on Γ_D). Newertheless, we have imposed a similar one ti the function v, but in a homogeneous way. As written now, data (f and g_1) are in the right-hand side and coefficients of the equation (the only one we have is c) are in the left-hand side. The expression on the left-hand side is linear in both u and v. It is a bilinear form of the variables u and v. The expression on the right-hand side is linear in v.

Without specifying spaces where u and v are, the weak formulation can be written as follows:

$$\begin{bmatrix} \textit{find } u \textit{ such that} \\ u = g_0 \quad on \ \Gamma_D \\ \int_\Omega \nabla u \cdot \nabla v + c \int_\Omega uv = \int_\Omega fv + \int_{\Gamma_N} g_1 v \end{bmatrix}$$

for all v, such that $v = 0$ on Γ_D.

Note how the two boundary conditions appear in very different places of this formulation:

1) The Dirichlet condition (given displacements) is imposed apart from the formulation and involves imposing it homogeneously to the testing function v. It is called an **essential boundary condition**.
2) The Neumann condition (given normal stress) appears inside the formulation. It is called a **natural boundary condition**.

3.4 The discrete variational problem

The finite element method (with linear finite elements on triangles) consists of the followinh discrete version of the proceding weak formulation:

$$
\left[
\begin{array}{c}
find\ u_h \in v_h\ \ such\ that \\
u_h(p) = g_0(p)\ \ for\ all\ Dirichlet\ node\ p \\
\int_\Omega \nabla u_h \cdot \nabla v_h + c\int_\Omega u_h v_h = \int_\Omega f v_h + \int_{\Gamma_N} g_1 v_h
\end{array}
\right.
$$

$\forall\ v_h\ \in\ V_h^{\Gamma_D}$

We have done trhee substitutions:

1) We look for the unknown in the space v_h instead of the whole Sobolev space. This mean that we have reduced the problem to computing u_h in the vertices of the triangulation (in the nodes) and we are left with a finite number of unknowns.

2) We have substituted the Direchlet condition by fixing the values of unknowns on dirichlet nodes. This fact reduces the number of unknowns of the system to the number of free nodes.

3) Finally, we have reduced the testng space from $H^1_{\Gamma_D}(\Omega)$ to its discrete subspace $V_h^{\Gamma_D}$. We will show right now that this reduces the infinite number of tests of the week formulation to a finite number of linear equations.

3.5 The associated system

We write again the discret problem, specifying the numbering of Dirichlet nodes in the discrete Dirichlet condition:

$$
\begin{bmatrix}
\text{find } u_h \in V_h, such\ that \\
u_h(p_j) = g_0(p_j)\ \forall j \in Dir \\
\int_\Omega \nabla u_h \cdot \nabla v_h + c\int_\Omega u_h v_h = \int_\Omega f v_h + \int_{\Gamma_N} g_1 v_h
\end{bmatrix}
$$

$$\forall V_h \in V_h^{\Gamma_D}$$

Our next claim is the following: the discrete equations

$$\int_\Omega \nabla u_h \cdot \nabla v_h + c\int_\Omega u_h v_h = \int_\Omega f v_h + \int_{\Gamma_N} g_1 v_h$$

$$\forall u_h \in V_h^{\Gamma_D}$$

are equivalent to the following set of equations

$$\int_\Omega \nabla u_h \cdot \nabla \varphi_i + c\int_\Omega u_h \varphi_i = \int_\Omega f \varphi_i + \int_{\Gamma_N} g_1 \varphi_i$$

$$\forall i \in Ind$$

Obviously this second group of equations is a small part of the originalo ne: it is enough to take $v_h = \varphi_1 \in V_h^{\Gamma_D}$. However, because of the linearity of the first expression in v_h, if we have the second for all φ_i, we the equaion for all possible linear combination of these functions, that is for all $v_h \in V_h^{\Gamma_D}$. Recapitulating, the method is equivalent to this set of N equations to determine the function u_h:

$$
\begin{bmatrix}
\text{find } u_h \in V_h, such\ that \\
u_h(p_j) = g_0(p_j)\ \forall j \in Dir \\
\int_\Omega \nabla u_h \cdot \nabla \varphi_i + \int_\Omega u_h \varphi_i = \int_\Omega f \varphi_i + \int_{\Gamma_N} g_1 \varphi_i
\end{bmatrix}
$$

$$\forall i \in Ind$$

To arrive to linear system, we have first to write u_h in terms of the nodal basis functions

$$u_h = \sum_{j \in Ind} u_j \varphi_j + \sum_{j \in Dir} u_j \varphi_j$$

Then we substitute the discrete Dirichlet condition in this expression

$$u_h = \sum_{j \in Ind} u_j \varphi_j + \sum_{j \in Dir} g_0(p_j) \varphi_j$$

Finally we plug this expression in the discrete variational equation

$$\int_\Omega \nabla u_h \nabla \varphi_j + c \int_\Omega u_h \varphi_i = \int_\Omega f \varphi_i + \int_{\Gamma_N} g_1 \varphi_i$$

apply linearity, noticing that

$$\nabla u_h = \sum_{j \in Ind} u_j \nabla \varphi_j + \sum_{j \in Dir} g_0(p_j) \nabla \varphi_j$$

and move to the right-hand side what we already know (the Dirichlet data)

$$\sum_{j \in Ind} \left(\int_\Omega \nabla \varphi_j \cdot \nabla \varphi_i \div c \int_\Omega \varphi_j \varphi_j \right) u_j$$
$$= \int_\Omega f \varphi_i + \int_{\Gamma_N} g_1 \varphi_1 - \sum_{j \in Dir} \left(\int_\Omega \nabla \varphi_j \cdot \nabla \varphi_i + c \int_\Omega \varphi_j \varphi_j \right) g_0(p_j)$$

This is a linear system with a many equations as unknows, namely with $Ind = \dim v_h^{\Gamma_D}$ equations and unknowns. The unknowns are in fact the nodal values of u_h on the free (non-Dirichlet) vertices of the triangulation. After solving this linear system, the formula for u_h lets us recover the function everywhere, not only nodes.

3.6 The wave equation

We will use homogeneous Dirichlet conditions in the entire boundary of the domain. The wave propagation problem is then

$$\begin{bmatrix} u_t = \Delta \times u + f & in \; \Omega \times (0, \infty) \\ u(\cdot, 0) = u_0 & in \; \Omega \\ u_t(\cdot, 0) = v_0 & in \; \Omega \\ u(\cdot, t) = o & on \; for \; all \; t > 0 \end{bmatrix}$$

If we try the finite difference in time approach, the simplest thing to do is to apply the central difference approximation to the second derivative. If we take a fixed time step, this means approximating

$$\phi''(t_n) \approx \frac{\phi(t_{n+1}) - 2\phi(t_n) + \phi(t_{t-1})}{\delta^2}$$

When applied to the time-variable in the wave equation we obtain the explicit time-step

$$\frac{u_{n+1} - 2u_n + u_{n-1}}{\delta^2} = \Delta u_n + f_n$$

After doing the weak formulation and introducing finite element spaces and beses, we end up with

$$M u_{n+1} = 2M u_n - M u_n - 1 - \delta^2 W u_n + \delta^2 f_n$$

The initial value for u_0 is easy. We still need u_1. For that, we can do very easy by taking a Taylor approximation

$$u_1 = u_0 + \delta v_0$$

or take a false discrete time -1 and use the equation

$$\frac{u_1 - 2u_0 + u_{-1}}{\delta^2} \Delta u_0 + f_0$$

to obtain the equation

$$\frac{u_1 - u_{-1}}{2\delta} v_0$$

together with the central difference approximation

$$u_1 = \frac{1}{2}\delta^2 \Delta u_0 + u_0 + \delta v_0 + \frac{1}{2}\delta^2 f_0$$

Then we need to give a weak formulation of this too. And do all the finite element stuff.

Introduction

The purpose of this work was to develop and to test a locating sources method of the volcanic tremor and to apply it at the existent dataset for Stromboli volcano.

For the location of the source, we used a locating procedure based on a probabilistic approach. The likelihood has been calculated through (by) a misfit function.

In fact, we looked for to locate the source of the tremor, whose location minimizes the error (mistake) between the observed amplitude and the calculate amplitude. The locating source of volcanic tremor has been represented by a distribution of probability over a regular grid of points 50 meter apart and frequency between 1 and 3 Hz. The inversion of the source has been performed in the frequency domain, using the amplitude of the wave field only. We have made the synthetic tests using sources with different depth and different configurations of the seismic networks.

4 Chapter

Application at Stromboli Volcano

4.1 Green's Function.

We developed a procedure to calculate the amplitude and phase of the wave field made by a source of tremor in a volcanic structure. Our purpose has been to simulate the wave field of volcanic tremor considering a complex topography. To able to perform the location of volcanic tremor in an enviroment with complex topography and to able to simulate the wave field in this situation, we needed some techniques for the calculation of Green's functions. We have decided to use the Element Finete Method (FEM) to calculate the Green's functions in the Fourier domain, because the elastodynamic Green's Functions are written like elliptic equations in the Fourier domain. The FEM is a suitable technique to resolve the problems kind elliptic. This method is particularly suitable when the boundary condition have some complex geometries. We considered an approximation of a point source where the signal wavelength is much greater than the distance between the source and receiver. The displacement field of the point source is :

$$U_k(t) = \sum F_i(t) * G_{ki}(t) + \sum \sum m_{ij}(t) * G_{ki,j}(t)$$

where the first term (zero-order) represents the single force while, the second term (one-order) represents the moment tensor components.

4.2 Finete Element Method (FEM).

The Finete Element Method (FEM) is a numerical technique suitable to look for an approximate solutions of problems described by differential equations. In our case, the differential equations are equations of second order partial differential. These equations are reduced to a system linear equations with the Finet Element Method. Our purpose has been to make a math model of a system, the geometry, the equations which rule the physical characteristics of this model, considering some boundary conditions. We consider the strong form of the equation:

$$-\nabla \cdot (a, \nabla u) = 0$$

and considering the following condition:

$$\int_{\Omega} L(u) \cdot v d\Omega$$

$$\forall V \in H_0^1$$

we obtain the weak form of the Laplace's equantion.

$$\int_{\Omega} \nabla u \cdot \nabla v dx + \int_{\Omega} u \cdot v + \int_{\partial \Omega} (\partial_n \cdot u) \cdot v = 0.$$

This equation is an integro-differential equation composed from volume-integrals and surface-integrals.

4.3 Example computation

The Green's function are calculated in the frequency domain, through a trhee-dimensional finet element method using the simulation software "Comsol multiphysics". We have imposted the Perfect Matched Layers (PML) boundary conditions the edges of the model (fig. 1). The discretized model has been done using the topography of Stromboli. The maximun elements size was chosen based on the minimum wavelength, related to the maximum frequency used (3Hz). The velocity model constists in a homogenueouse medium with compressional wave velocity $Vp = 3.5\ Km/s$ and ${Vp}/{Vs} = \sqrt{3}$ (Fig). For our porpuse, the Green's Function are obtained for a point source positioned over a grid nodes spaced 50 m apart (Fig. 2).

$$U_k(\omega) = m_{ij}(\omega) \cdot G_{ki,j}(\omega)$$

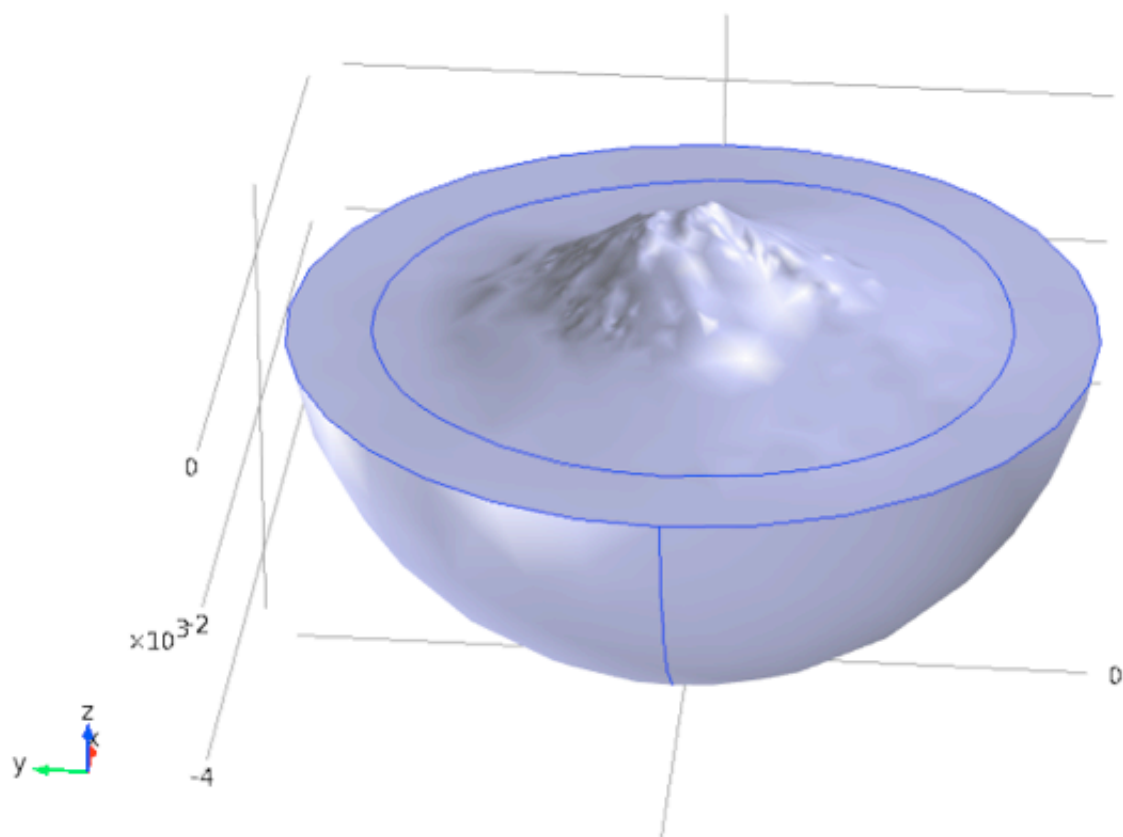where $U_k(\omega)$ rapresent the displecement field in the frequency domain.
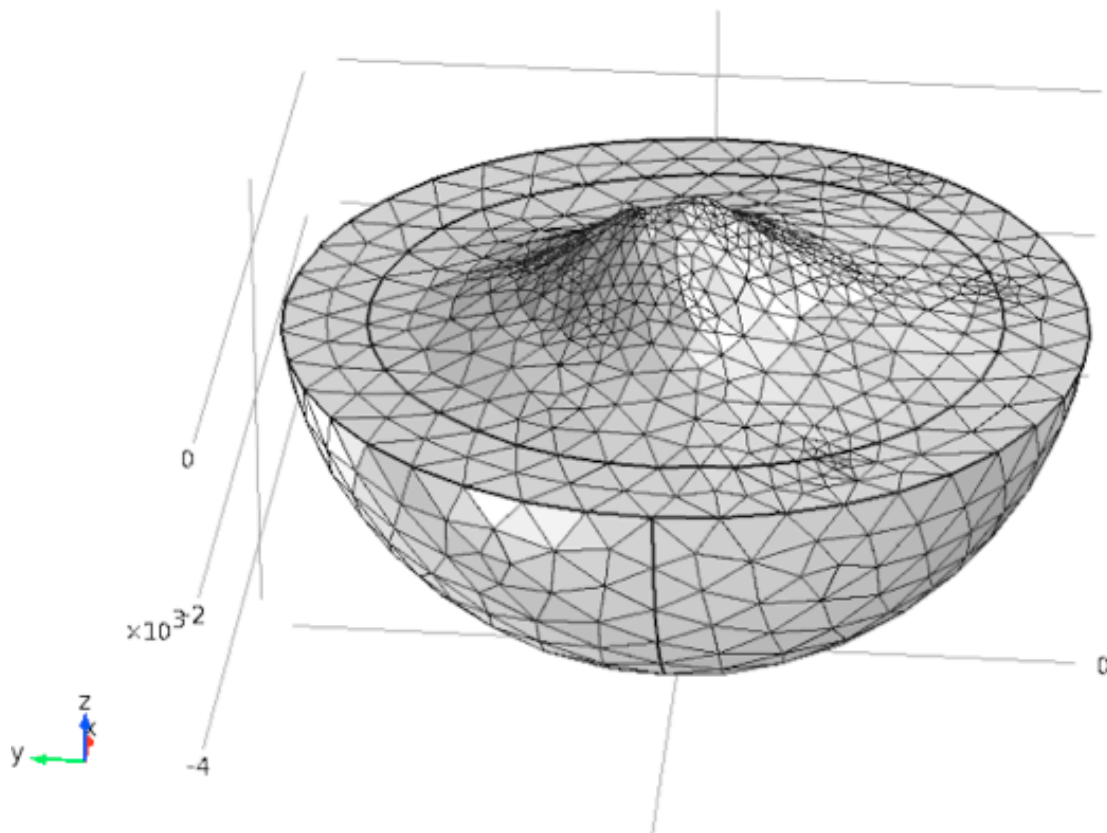
Fig. 1 Stromboli Geometry

Fig. 2 Tetrahedral Mesh

This model has been developed considering two boundary conditions: 1) Neumann's condition, 2) Dirichlet's condition. The Neumann's condition imposes the derivative of the normal function has to assume a value on the edge of the surface. In our case, this condition has been used to assume the cancellation condition of the normal stress of the free surface. On the other hand, the Dirichlet's condition, for our purpose, has been assumed fixed where the displacement over the surface is 0. We have used this condition because we need to specify a condition over the free surface to ensure stability to the solution (the condition imposes that the volume is stopped also if there is a force which acts on the source). Anyway, this condition is appropriate to mold the wavefield, because the wavefield decays before it arrives to the external edge, because it is damped by the Perfect Matched Layers (PML). The PML is an additional domain where the alastodynamic equations change. In this way, the waves have an exponential decay in a particular direction. We choose a spherical model because the direction of the decay is radial.

Below we show the results of Green's Function $G_{zz,x}$ calculated for a source with 500 m of elevation and 2 Hz of frequency (Fig. 3)
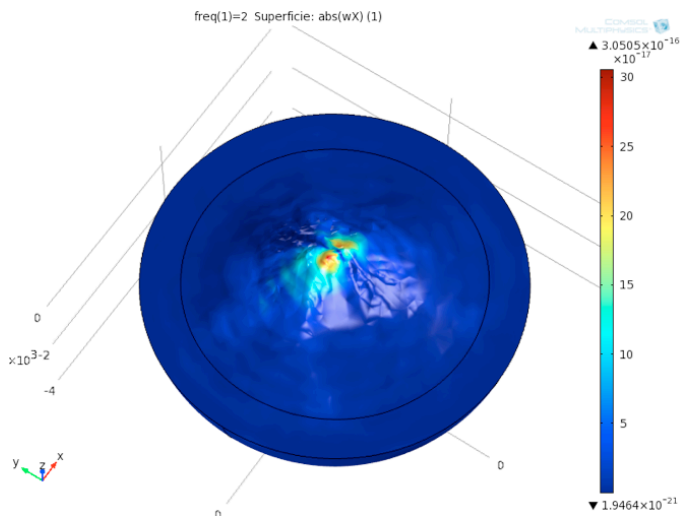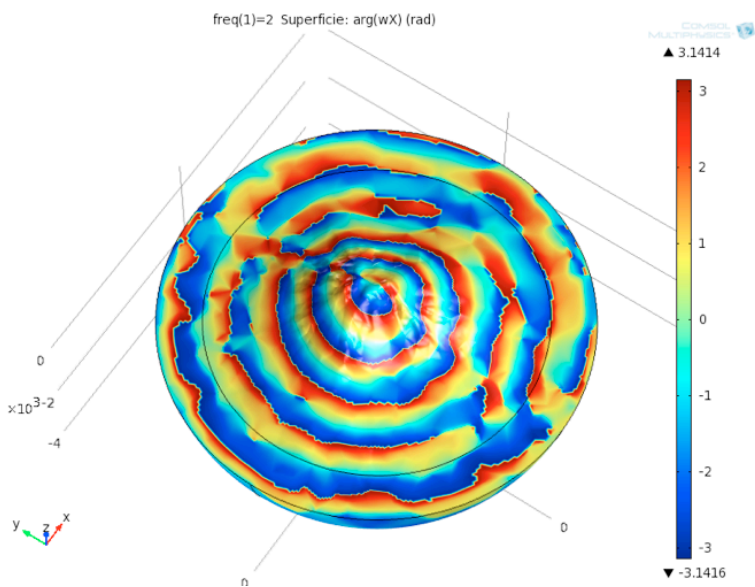
Fig. 3   Up: Absolute value. Considerable effect of the topography over the wavefield. The amplitudes are concentraded on the concavity of "La Sciara del Fuoco".
Down: Green's Function phase.

4.4 Location of the source.

For location of the source of the volcanic tremor, we used a probabilistic approach. We calculated a theoric source using a simple last square approach:

$$S^{TH} = \frac{\sum_{i=1}^{N} d_i(f) G_i^{iso}(f)}{\sum_{i=1}^{N} G_i^{iso}(f)^2}$$

where N is the number of channels, G_i^{iso} is the Green's Function generalized for an isotropic source, d are the observed data and f is the frequency.

Then, we calculated the misfit function for every point of the regular grid:

$$E(x,y,z) = \frac{\sum_{i=1}^{N} \sum_{j=1}^{F} [d_i f_j - d_i^{TH}(f_j)]^2}{\sigma^2}$$

using a probabilistic approach, to assess the location quality, we have:

$$p \propto e^{-E}$$

where p is our probability function and E is our misfit function. The probability function then is normalized, so we have:

$$p = \frac{p}{\int_v p \, dv}$$

4.5 Synthetic tests.

We made synthetic tests, using sources with various depth, different network configurations, with frequencies between 1 and 3 Hz and a flat amplitude spectrum. With increasing of the depth of the source and with the decreasing of the stations, the probability function worsens. Despite it, the location seemes to be quite accurate.

In figures 4, 5,6,7,8, 9 are rapresented the probability distribution. The red points indicate the seismic stations of the network, the blu stars represents he volcanic tremor source.
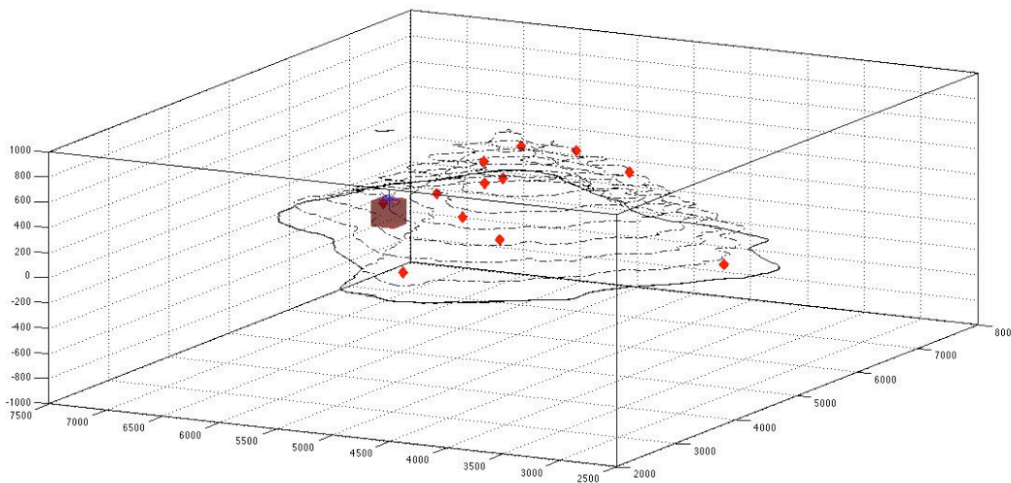

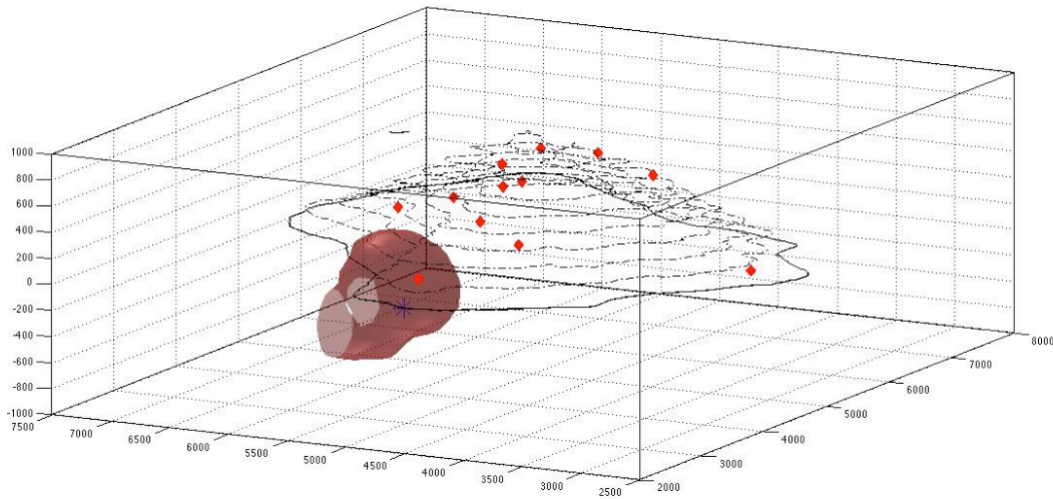Fig. 4 12 stations, 99% confidence volume, elevation 400 m.

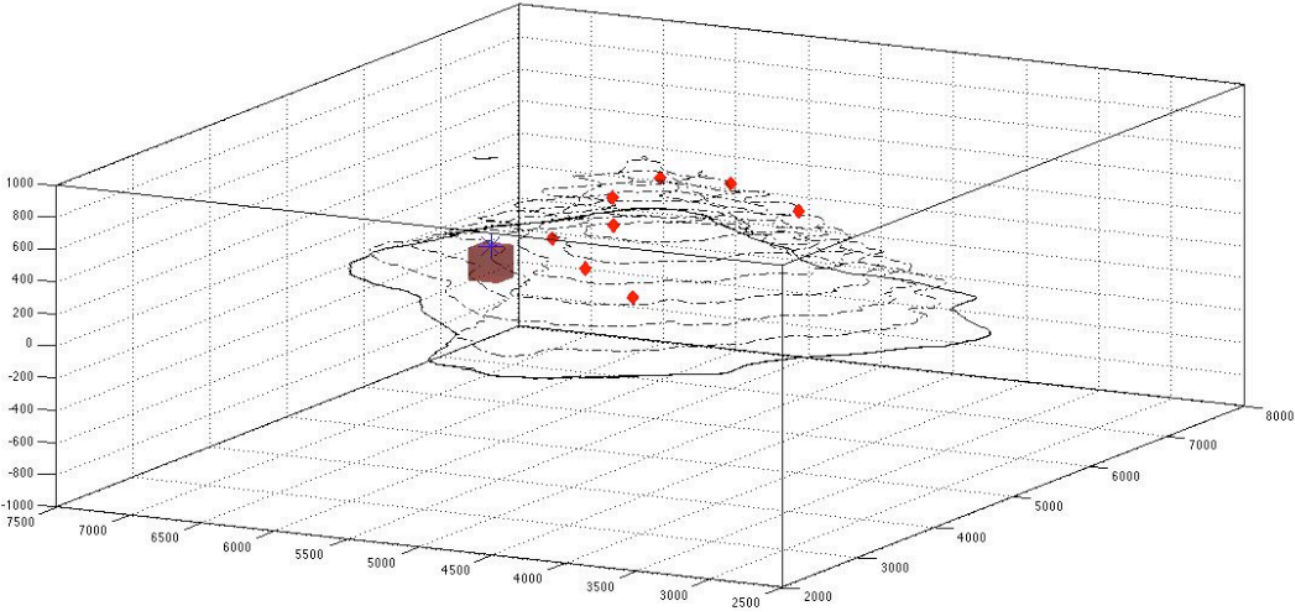Fig. 5   12 stations, 99% confidence volume, elevation -400 m.

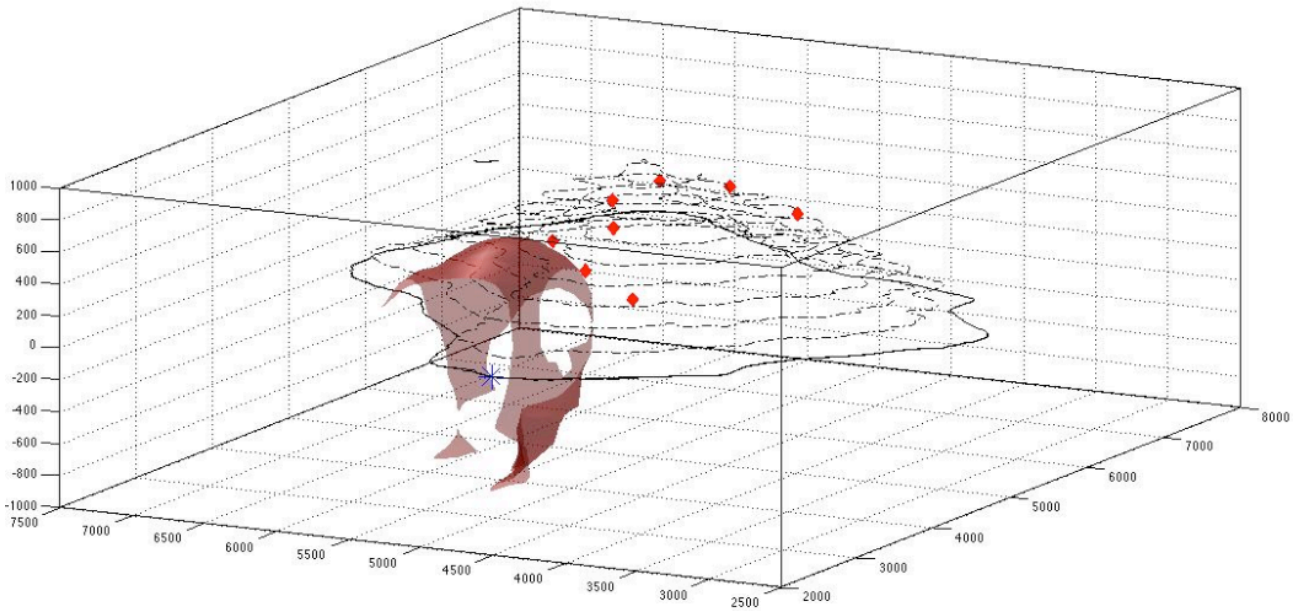Fig. 6   8 stations, 99% confidence volume, elevation 400 m

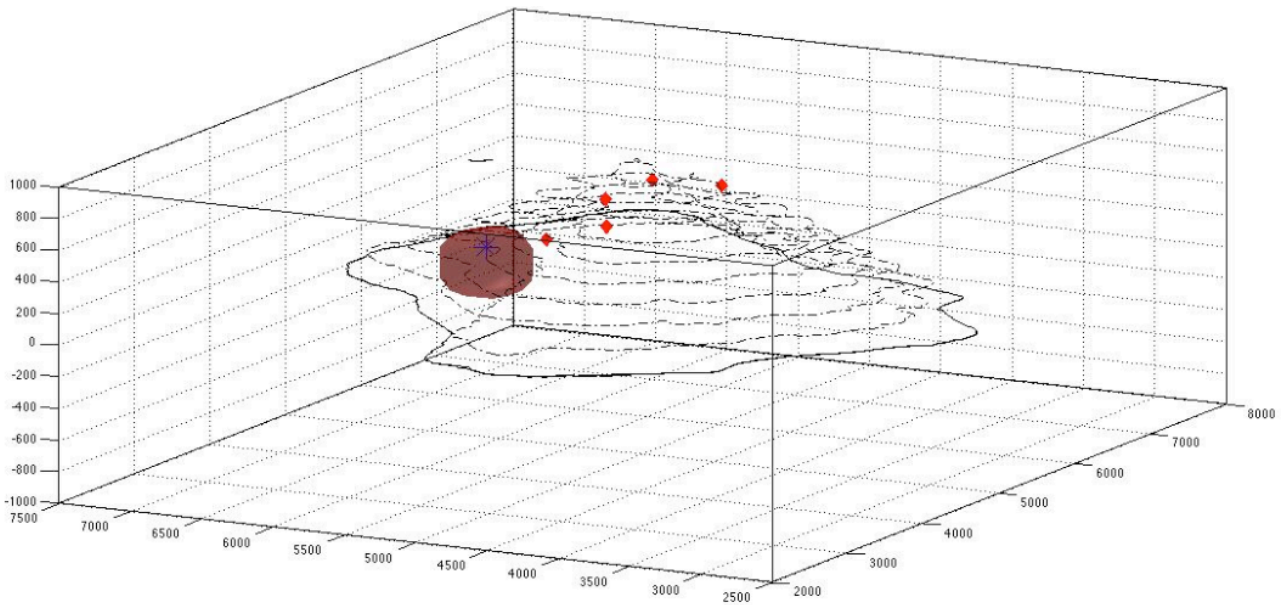Fig. 7 8 stations, 99% confidence volume, elevation -400

Fig. 8 6 summit stations, 99% confidence volume, elevation 400 m.
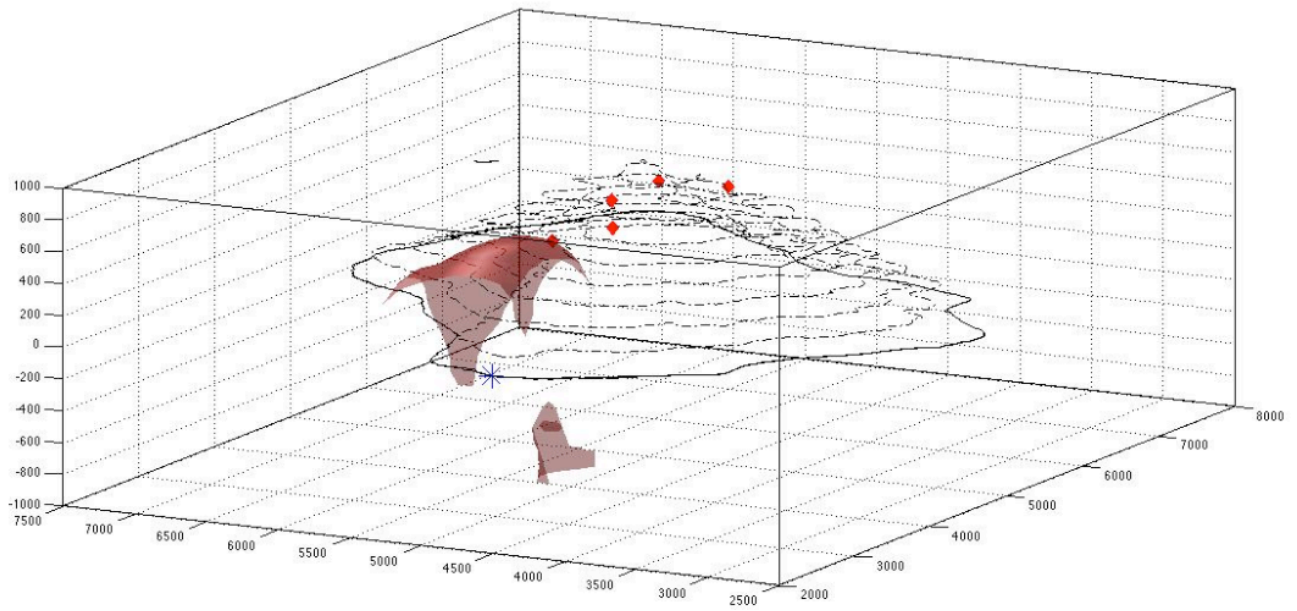
Fig. 9 6 summit stations, 99% confidence volume, elevation -400 m.

4.6 Stromboli dataset

On February 27, 2007, by about 09:00 UTC, a landslide signal was seen by the analysts involved in the sourveillance activity. At 12:34 UTC, the volcano started the effusive phase, and at 12:39 UTC a stronger landslide seismic signal was recorded. The lava flowed from a fracture that opened in the North-East crater, down the "La Sciara del Fuoco" flank. With the beginning of the lava flow, the explosive activity at the summit vents ceased. In the first few hours of the effusive phase, the tremor amplitude showed two episodes of strong incrementation and the nit dropped down a very low level. These two episodes have distinctive spectral features that make them clearly distinguishable from the common volcanic tremor. One of the most interesting feature is that the amplitude was maximum at the STR8 station (located close to the "La Sciara del Fuoco").

The method was able to locate the volcanic tremor sources at Stromboli. The non-linear probabilistic approach is well suited for this task. The multiple tremor sources have been identified at Stromboli during on February 27, 2007, eruption. The changes in the source location may reflect the emptying of the shallow volcanic conduit during the lava flow.

Before the effusive phase, the source is located under the summit craters along "La Sciara del Fuoco" (Fig. 10).

After the effusive phase, there are three relative maxima of the probability distribution. These could be linked to three different sources: one is located near the craters, one close to the lava flow vent and the last one is deepest (FIg. 11).
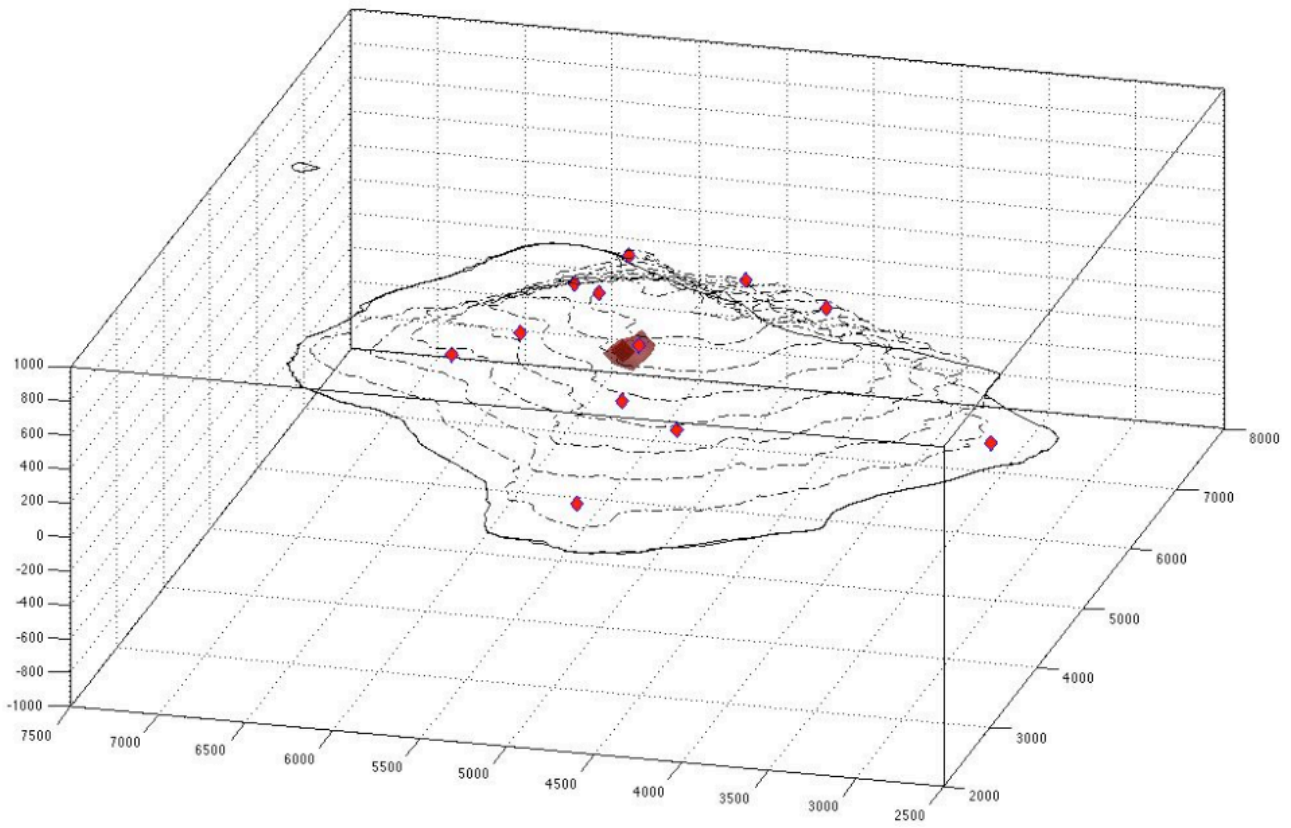
Fig. 10   Before the effusive phase: Time 00:05 UT, Window lenght 20:48 s, Frequency 1-3 Hz, 12 Stations, 90% Confidence volume.
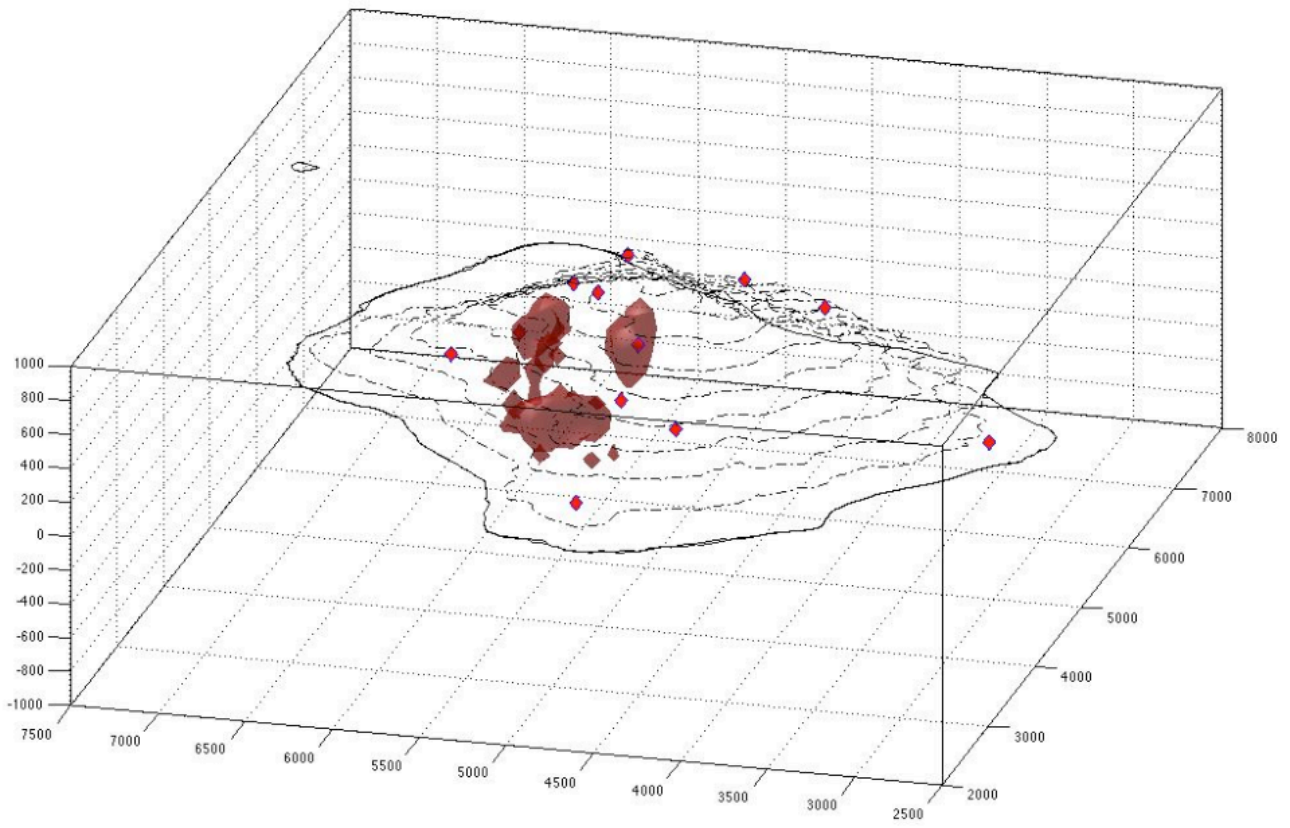
Fig. 11   After the effusive phase: Time 23:40 UT, Window lenght 20:48 s, Frequency 1-3 Hz, 90% Confidence volume.

Conclusions

The purpose of this work is to develop a method for locating volcanic tremor sources. This method will be applaied on Stromboli vulcano dataset (7 years of recods). The work will concentrate mostly identifyng the number and location of the sources investigating on their temporal variation.

Volcanic tremor has attracted considerable attention by seismologist because of its potential value as a tool for forecasting eruptions and better understanding the physical processes that occur inside active volcanoes. However, unlike tectonic earthquakes where the dominant source process is brittle failure of rock, the driving mechanism of tremor seems to involve complex interactions of magmatic fluids with the surrounding bedrock. These interactions are responsible for the following distinct characteristics found in volcanic tremor recorded at many volcanoes worldwide: a) the onset of tremor may be emergent or impulsive, with its amplitude showing in many cases a dirct relationship the volcanic activity; b) in the frequency domain the spectra consist of a series of sharp peaks in the band 0.1-7 Hz, representing either a fundamental frequency and its harmonics, or a random distribution, while quite often they exhibit temporal variations in their content; c) the depth of the source can very considerably from one volcano to another in the range of a few hundred metres to 40 km; d) tremor may occur prior to and/or after eruptions with a duration that ranges from several minutes to several days or months. The methods used to study tremor include spectral analysis using both the Fast Fourier

Transformation and the Maximum Entropy Method, polarisation analysis of the wavefield and methods that make use of array data to deduce the backazimuth and type of the seismic waves as well as the location of the source. Visual and/or recorded acoustic observations of the ongoing volcaanic activity have assisted in many cases to further constrain proposed physical mechanisms for the generation of tremor. The models suggested as possible sources of tremor can be grouped as follows: a) fluid flow induced oscillations of conduits transporting magmatic fluids; b) excitation and resonance of fluid-filled cracks; c) bubble growth or collapse due to hydrothermal boiling of groundwater; d) a variety of models involving the oscillations of magma bodies with different geometries. It has been proposed by many authors that the source of tremor is not unique and may differ from one volcano to another, a fact that adds mor difficulty in the source modelling efforts.

Most methods used to locate volcanic tremor sources are: 1) use of array, 2) the calculation of wave field amplitude. The study on volcanic tremor for Stromboli volcano will be carried out adopting the latter basing the method on a realistic wavefield model.

On February 27, 2007, by about 09:00 UTC, a landslide signal was seen by the analysts involved in the sourveillance activity. At 12:34 UTC, the volcano started the effusive phase, and at 12:39 UTC a stronger landslide seismic signal was recorded. The lava flowed from a fracture that opened in the North-East crater, down the "La Sciara del Fuoco" flank. With the beginning of the lava flow, the explosive activity at the summit vents ceased. In the first few hours of the effusive phase, the tremor amplitude showed two episodes of strong incrementation and the nit dropped down a

very low level. These two episodes have distinctive spectral features that make them clearly distinguishable from the common volcanic tremor. One of the most interesting feature is that the amplitude was maximum at the STR8 station (located close to the "La Sciara del Fuoco").

The method was able to locate the volcanic tremor sources at Stromboli. The non-linear probabilistic approach is well suited for this task. The multiple tremor sources have been identified at Stromboli during on February 27, 2007, eruption. The changes in the source location may reflect the emptying of the shallow volcanic conduit during the lava flow.

Before the effusive phase, the source is located under the summit craters along "La Sciara del Fuoco".

After the effusive phase, there are three relative maxima of the probability distribution. These could be linked to three different sources: one is located near the craters, one close to the lava flow vent and the last one is deepest.

The future developments could be: to include the attenuation factor to employ this method at volcanic structures bigger like Kilauea volcano, Etna volcano; to consider complex sources; to employ the method in real time.

References

J.P. Benoit, S. McNutt, V. Barboza. Duration-amplitude distribution of volcanic tremor. Journal of Geophys. Res.,108, B3(2146), 2003.

R.J. Bruce. Volcanic tremor: Nonlinear excitation by fluid flow. Journal of Geophys. Res., 99:859-877, 1994.

B. Chouet. Exicitation of a buried magmatic pipe: A seismic source model fo volcanic tremor. Journal of Geophys. Res., 90:1881-1893, 1985.

B. Chouet. Volcano seismology. Pure appl. Geophys., 739-788, 2003.

M.G. Ferrick, A. Qumar, W.F. St. Lawrence. Source Mechanism of volcanic tremor. Journal of Geophys. Res., 87:8675-8683, 1982.

E. Gordeev, V.A. Saltykov, V.I. Sinitsyn, V.N. Chebrov. Temporal and spatial characteristics of volcani tremor wave fields. Journal of Volcanol. Geotherm. Res., 40:89-101, 1990.

E.I. Gordeev. Modelling of volcanic tremor wave fields. Journal of Geotherm. Res.., 51:145-160, 1992.

S. Honda, K. Yomogida. Periodic magma movement in the conduit with a barrier: a model for the volcanic tremor. Geophys. Res. Lett., 20:229-232, 1993.

A.W. Hurst. A volcanic tremor monitoring system. Journal of Geotherm.res., 26:181-187, 1985.

Y. Ida. Cyclic fluid effusion accompanied by presure change: implication for volcanic eruptions and tremor. Geophys. Res. Lett., 23:1457-1460, 1996.

I. Lokmer, G.S. O'Brien, D. Stich, C.J. Bean. Time reversal imaging of synthetic volcanic tremor sources. Geophys. Res. Lett., 36, L12308, 2009.

B. Martinelli. Volcanic tremor and short-term prediction of eruptions. Journal of Volcanol. Geotherm. Res., 77:305-311, 1997.

M. Martini, F. Giudicepietro, T. Caputo, R. Curciotti, W. De Cesare, M. Orazi, G. Scarpato, R. Peluso, P. Ricciolino, A. Linde, S. Sacks. Sesmological monitoring of the february 2007 effusive eruption of the stromboli volcano. Annals of Geophys., vol 50, 2007

S. McNutt, T. Nishumura. *Volcanic tremor during eruptions: temporal characteristics, scaling and constraints on conduit size and processes. Journal of Volcanol. Geotherm. Res., 178:10-18, 2008.*

K.I. Kostantinou, V. Schlindwein. *Nature, wavefield properties and source mechanism of volcanic tremor: a review. Journal of Volcanol. Geotherm. Res., 119:161-187, 2002.*

R. Schick. *Volcanic tremor-source mechanisms and correlation with eruptiv activity. Nature Hazard, 1:125-144, 1988.*

G.S. Steinberg, A. S. Steinberg. *On possible causes of volcanic tremor. Journal of Geophys. Re., 80, 11, 1975.*

S. Alparone, D. Andronico, L. Lodato, T. Sgroi. *Relationship between tremor and volcanic activity during the southeast crater eruption on mount etna in early 2000. Journal of Geophys. Res., 108, B5, 2003.*

J. Battaglia, K. Aki. *Location of seismic events and eruptive fissures on the piton de la fournaise volcano using seismic amplitudes. Journal of Geophys. Res., 108, B8, 2003.*

J. Battaglia, K. Aki, V. Ferrazzini. *Location of tremor sources and stimation of lava output using tremor source amplitude on the Piton de la Fournaise volcano: location of tremor sources. Journal of Volcanol. Geotherm. Res., 147:268-290, 2005.*

A. Cannata, G. Di Grazia, P. Montalto, F. Ferrari, G. Nunnari, D. Patanè, E. Privitera. *New insights into banded tremor from the 2008-2009 mount etna eruption. Journal of Geophys. Res., 115, B12318, 2010.*

A. Cannata, A. Catania, S. Alparone, S. Gresta. *Volcanic tremor at mt. Etna: inferences on magma dynamics during effusive and explosive activity. Journal of Volcanol. Geotherm. Res., 178:19-31, 2008.*

E. Fujita. *Banded tremor at mijakejima volcano, japan: implication for two-phase flow instability. Journal of Geophys. Res., 113, B04207, 2008.*

M. Furumoto, T. Kunimoto, H. Inoue, I. Yamada, K. Yamaoka, A. Ikama, Y. Fukao. *Twin sources of high-frequency volcanic tremor of izu-oshima volcano, japan. Geophys. Res. Lett., 17:25-27, 1990.*

M. Riuscetti, R. Schick, D. Seidel. *Spectral parameters of volcanic tremors at etna. Journal of Volcanol. Geotherm. Res., 289-298, 1977.*

G. Saccorotti, B. Chouet, P. Dawson. Shallow-velocity models at kilauea volcano, hawaii, determined from array analyses of tremr wavefields. Geophys. J. Int., 633-648, 2003.

G. Saccorotti, B. Chouet, P. Dawson. Wavefield properties of a shallow long-period event and tremor at kilauea volcano, hawaii. Journal of Volcanol. Geotherm. Res., 163-189, 2011.

N. Takagi, S. Kaneshima, T. Ohkura, M. Yamamoto, H. Kawakatsu. Long-term variation of the shallow tremor sources a taso-volcano from 1999-2003. Journal of Volcanology and Geotherm. Res., 333-346, 2009.

N. Takagi, S. Kaneshima, H. Kawakastu, M. Yamamoto, Y. Sudo, T. Ohkura, S. Yoshikawa, T. Mori. Apparent migration of tremor source synchronized with the change in the tremor amplitude observed a taso volcano, japan. Journal of Volcanol. Geotherm. Res., 181-200, 2006.

R. Carniel, M. Tarraga. Can tectonic events change volcanic tremor at stromboli? Geophys. Res. Lett., L20321, 2006.

B. Chouet, G. De Luca, G. Milana, P. Dawson, M. Martini, R. Scarpa. Scallow velocity structure of stromboli volcano, italy, derived from small-aperture array measurements of strombolian tremor. Bulletin of Seismol. Society of America, 88:653-666, 1998.

B. Chouet, G. Saccorotti, P. Dawson, M. Martini, R. Scarpa, G. De Luca, G. Milana, M. cattaneo. Broadband measurements of the sources of explosions at stromboli vulcano, italy. Geophys. Res. Lett., 26:1937-1940, 1999.

S. Falsaperla, H. Langer, S. Spampinato. Statistical analyses and characteristics of volcanic tremor on stromboli volcano (italy). Bull Volcanol, 60:75-88, 1998.

J.M. Ibanez, C. Benitez, L.A. Gutierrez, G. Cortes. The classification of seismo-volcanic signals using hidden morkov model sas applied to the stromboli and etna volcanoes.

H. Langer, S. Falsaperla. Long-term observation of volcanic tremor on stromboli volcano (italy): a synopsis. Pageoph, vol. 147, 1996.

M. Ripepe, P. Poggi, T. Braun, E. Gordeev. Infrasonic waves and volcanic tremor at stromboli. Geophys. Res. Lett., 23:181-184, 1996.

M. Ripepe. Gas bubble dynamics model for shallow volcanic tremor at stromboli. Journal of Geophys. Res., 10:639-652, 1999

F.Fattori Speranza, R. Carniel. Structural changes of volcanic tremor at stromboli volcano. Journal of Vulcanol. Geotherm. Res., 103-117, 2008.

L. Telesca, M. Lavallo, R. Carniel. Time-dependent fisher information measure of volcanic tremor before the 5 april 2003 paroxysm at stromboli volcano, italy. journal of Vulcanol. Geotherm. Res., 78-82, 2010.

P. Dawson, B. Chouet, P. Okubo, A. Villasenor, A.H.M. Benz. Three-dimensional velocity structure of the kilauea caldera, hawaii, Geophys. Res. Lett., 2805-2808, 1999.

P. Goldestein, B. Chouet. Array measurements and modeling of sources of shallow volcanic tremor at kilauea volcano, hawaii. Journal of geophys. Res., 2637-2652, 1994.

S. McNutt, S. Ida, B. Chouet, P. Okubo, J. Oikawa, G. Saccorotti. Kilauea volcano provides hot seismic data for joint jaanese-us experiment. EOS, Trans. Am. Geophys. Un., 105-107, 1997.

P. Okubo, H.M. benz, B. Chouet. Imaging the crustal magma sources beneath mauna loa and kilauea volcanoes, hawaii. Geology, 867-870, 1997.

J. Almendros, J.M. Ibanez, G. Alguacil, E. Del Pezzo, R. Ortiz. Array tracking of the volcanic tremor source at deception island, antartica. Geophys. Res. Lett., 3069-3072, 1997.

J. benoit, S. McNutt. New constraints on the source processes of volcanic tremor at arenal volcano, costa rica., using broadband seismic data. Geophys res. Lett., 449-452, 1997.

M.C. Fehler. Observations of volcanic tremor at mt st. elens volcano. Journal of Geophys. Res., 3476-3484, 1983.

V. Ferrazzini, A. Aki, B. Chouet. Characteristics of seismic waves composing hawaiian volcanic tremor and gas-piston events observed by a near source array. Journal of Geophys. Res., 6199-6209.

A.S. Hofstetter, S. Malone. Observations of volcanic tremor at mt. St. elens in april and may 19980. Bull. Seismol. Soc. Am., 923-938, 1986.

K. Aki, M. Fehler, S. Das. Source mechanism of volcanic tremor: fluid driven crack models and their application to the 1963 kilauea eruption. Journal of Volcanol. Geotherm. Res., 259-287, 1977.

B. Chouet,. Resonance of a fluid-driven crack: radiation properties and implications for the source of long-period events and harmonic tremor. Journal of Geophys. Res., 4375-4400, 1988.